Nucleic Acids Research, 2025, **53**, gkaf211
https://doi.org/10.1093/nar/gkaf211
Gene regulation, Chromatin and Epigenetics

SMARCA4 regulates inducible BRD4 genomic redistribution coupling intrinsic immunity and plasticity in epithelial injury-repair

Xiaofang Xu[1] **and Allan R. Brasier**[1,2,*]

[1]Department of Medicine, University of Wisconsin–Madison School of Medicine and Public Health (SMPH), Madison, WI 53705, United States
[2]Institute for Clinical and Translational Research, University of Wisconsin–Madison, Madison, WI 53705, United States

[*]To whom correspondence should be addressed. Tel: +1 608 263 7371; Email: abrasier@wisc.edu

Abstract

Coordinated expression of differentiation and innate pathways is essential for successful mucosal injury-repair. Previously, we discovered that the core SWI/SNF complex ATPase, SWI/SNF-related, matrix associated, actin dependent regulator of chromatin, subfamily A, member 4 (SMARCA4)/Brg1, maintains tumor protein 63 + basal progenitor cells in an epithelial-committed state. In response to viral injury, SMARCA4 complexes BRD4 to activate innate inflammation and promote mesenchymal transition/plasticity. To investigate how innate inflammation couples with plasticity, Cleavage Under Targets and Release Using Nuclease of BRD4 binding was applied to wild type and SMARCA4 knockdown (KD) in mock- or respiratory syncytial virus (RSV)-infected basal cells. In mock-infected cells, BRD4 binds 4017 high-confidence peaks within gene bodies controlling mesenchymal transition pathways. By contrast, RSV replication repositions 2339 BRD4 peaks to open chromatin regions upstream of the genes controlling inducible cytokine, cell adherence, and antiviral programs. Also, we note RSV redistributes BRD4 into super enhancers regulating immune response-associated long noncoding (lnc)RNAs. In SMARCA4 KD cells, BRD4 distribution is reduced on 739 peaks after RSV infection. The boundaries of nucleosome-free regions are reduced by SMARCA4 KD, suggesting its role in maintaining open chromatin of super enhancers. Specifically, SMARCA4–BRD4 enhancer controls lncRNAs important in interferon response factor 1 autoregulation. These data indicate how SWI/SNF ATPases couple BRD4 to lncRNA expression controlling cell state and intrinsic immunity in epithelial injury-repair.

Graphical abstract

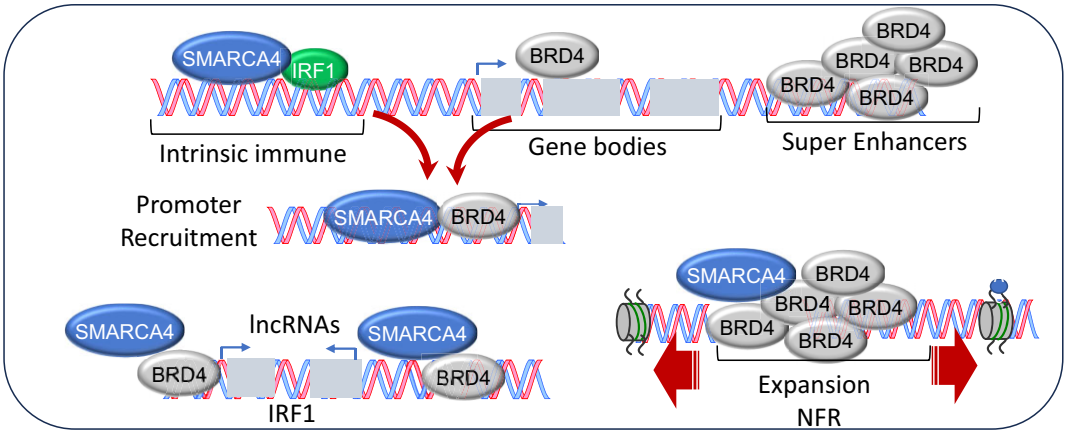

Introduction

The terminally differentiated airway epithelium is a pseudostratified tissue that forms a semi-impermeable barrier preventing inhaled particles and microbes from gaining access to the interstitial space [1]. When this critical barrier surface is disrupted by exposure to environmental toxicants and/or viral pathogens [1], multipotent progenitors within the basal layer activate a stereotypic cellular stress-response program to repopulate the denuded surface. Transient or limited epithelial injury involves induction of innate immune defenses, cellular de-differentiation, and activation of motility enabling surviving basal cells to repopulate the airway, restoring physical and immunological homeostasis [2]. By contrast, persistent injury results in stem cell depletion, dysfunctional epithelial differentiation, cellular senescence, and tissue dysplasia [3–6]. Disorders associated with chronic, repetitive injury are associated

Received: October 1, 2024. **Revised:** February 25, 2025. **Editorial Decision:** February 28, 2025. **Accepted:** March 6, 2025

with common environmental-induced lung diseases, including chronic obstructive airway diseases, asthma and chronic obstructive pulmonary disease (COPD), that collectively are responsible for clinical disease affecting 600 million patients [7], responsible for one-third of preventable deaths and incur health expenditures of $326 trillion dollars globally [8]. A better understanding of how injury-repair pathways are controlled is urgently needed.

Multipotent tumor protein 63 (TP63)- and keratin 5(KRT5)-expressing human small airway epithelial cells (hSAECs) in the basal membrane play central roles in airway regeneration [9]. This cell population is epigenetically programmed to de-differentiate into motile mesenchymal cells via partial epithelial mesenchymal transition (also known as "plasticity" [10–12]). Here, viral infection or stimulation with epithelial growth factors induces gene expression programs controlling mesenchymal transition, including activation of the core mesenchymal transcription factors, snail family transcriptional repressor 1 (SNAI1) and the zinc finger E-box binding homeobox 1 (ZEB1) [11], upregulation of mesenchymal contractile proteins (Vimentin) [11], formation of actin stress fibers [13], secretion of extracellular matrix components [13], and loss of epithelial tight junctions (TJs) [13]. This complex, coordinated response to airway injury enables de-differentiated basal epithelial cells to repopulate the airway to restore normal airway barrier.

In addition, basal cells exhibit relative resistance to viral infection by constitutively expressing an intrinsic innate immune response (IIR) [14, 15]. The intrinsic IIR is an interferon (IFN) response factor 1 (IRF1)-dependent gene network that provides broad antiviral protection by maintaining IFN-responsive genes (ISGs) in a highly inducible state [14, 16–20]. When activated, the innate signaling pathway reprograms intracellular glucose metabolism, induces plasticity, and coordinates extracellular matrix secretion [11, 21, 22]. The regulatory mechanisms controlling how innate signaling is coupled with these dynamic phenotypic transitions are not fully understood.

Basal cells are multipotent, lineage-restricted cells capable of self-replication as well as transitioning into terminally differentiated epithelium of multiple types [18, 23]. These properties are regulated by complex epigenetic modifications regulating enhancer–promoter contacts and chromatin conformation [24]. Although multiple lineage-dependent activators and repressors participate in establishing multipotency, these interactions involve the activity of bromodomain (BD)-containing nucleosome-positioning ATPases and acetyl lysine binding histone acetyltransferases (HATs). Differential chromatin conformation assays and RNAi screening studies have shown that SWI/SNF-related, matrix associated, actin dependent regulator of chromatin, subfamily A, member 4 (SMARCA4) is a primary regulator of chromatin relaxation, influencing self-renewal and differentiation. Currently it is recognized that SMARCA4 is a pleiotropic chromatin regulatory protein that not only displaces nucleosomes during inducible transcription [25], but also antagonizes polycomb repression [26], relaxes chromatin during the DNA damage-repair response [27], supports 3D chromatin conformation [28], and forms a protein component of structural nuclear bodies [28]. In addition, we found that SMARCA4 was a repressor of de-differentiation, where in the absence of SMARCA4, basal cells entered unscheduled plasticity and secreted enhanced extracellular matrix-remodeling factors [13].

Acting in concert with SMARCA4, bromodomain-containing protein 4 (BRD4) is an atypical HAT that maintains higher order chromatin structure [29], supporting stable cell identity [30] and required for inducible transcription [31, 32]. Through formation of protein–protein complexes with epithelial lineage-determining transcription factors, BRD4 promotes terminal differentiation through the formation of "super enhancers" maintaining expression of lineage controlling factors [30]. In response to growth factor signaling, BRD4 complexes with cyclin-dependent kinases [33] and acetylated transcription factors to promote transcriptional elongation [34] of immediate-early genes, extracellular matrix, and growth factors during epithelial injury-repair [35, 36]. The inducible targeting of BRD4 to chromatin is complex, mediated by BRD4 BD interactions with inflammation-activated transcription factors such as NFκB and IRF1 [15, 32, 37], as well as acetylated histones [31]. A more comprehensive understanding of the mechanisms controlling regulation of BRD4 activation and chromatin targeting will be of significant importance in understanding epithelial determination.

Respiratory syncytial virus (RSV) infections are the major human pathogens that directly target differentiated epithelial cells, producing sloughing, barrier dysfunction, and exacerbations of chronic respiratory disease [38–44]. Relatively resistant to RSV infection, upon infection, basal epithelial cells activate the unfolded protein response producing metabolic reprogramming of hexosamine biosynthesis [14, 15, 21, 45–47]. These programs are permissive to express mesenchymal contractile proteins and secrete extracellular matrix promoting repair. Although the individual roles of SMARCA4 and BRD4 in inducible stress response pathways have been studied in some detail, the mechanisms how these factors cooperate to couple the intrinsic IIR with plasticity are not understood.

Here, we discover that SMARCA4 complexes are engaged with IRF1 priming the core intrinsic IIR genes. In response to viral replication, SMARCA4 complexes with BRD4, whose activity is required for coupled intrinsic IIR and plasticity programs. To determine if SMARCA4 regulates BRD4 binding, we determined BRD4 genomic distribution using Cleavage Under Targets and Release Using Nuclease (CUT&RUN) assays in SMARCA4 wild-type (WT) and knockdown (KD) cells. In unstimulated WT cells, BRD4 is localized to gene bodies, but repositions to regulatory regions in proximal promoters and super enhancers. By contrast, in SMARCA4 KD cells, a subset of BRD4 binding is reduced to proximal promoters and super enhancers. These include promoters expressing nuclear paraspeckle assembly transcript 1–2 (*NEAT1–2*) and *Interferon stimulated response 8 (ISR8)/IRF1-antisense (IRF1-AS)* lncRNAs regulating nuclear bodies and intrinsic immunity. These findings indicate that SMARCA4 is a factor controlling BRD4 dynamical chromatin repositioning coordinating intrinsic immunity and epithelial plasticity in injury-repair.

Materials and methods

Cell cultures and siRNA transfection

Telomerase-immortalized primary human Small Airway Epithelial Cells (hSAECs) were grown in small airway epithelial cell growth medium (Lonza, Walkersville, MD, USA) in 5% CO_2. Sucrose cushion-purified RSV long strain was used to infect hSAECs at an multiplicity of infection (MOI) of 1.0

[11, 13]. The BRD4 inhibitor ZL0454 was used at 10 μM concentration [48].

RNA isolation and quantitation

Total cellular RNA was extracted with RNeasy kit (Qiagen 75144). For real-time polymerase chain reaction (qRT-PCR), complementary DNA were synthesized with LunaScript RT supermix kit (NEB E3010) and amplified with NEBNext high-fidelity 2× PCR master mix (NEB M0541). Gene-specific primer sequences are from [15] and shown in Supplementary Table S1. Quantification of relative changes in gene expression was calculated using the ΔΔCt method and normalized to internal control PPIA.

For RNA sequencing (RNA-seq), RNA was quantified (Nanodrop) and integrity verified (Agilent) prior to sequencing. To determine effect of SMARC KD, 24 separate RNA samples ($N = 4$ each for hSAEC and SMARCA4 KD cells at time 0, 16, and 24 h of RSV treatment) were bar-coded and subjected to Illumina HiSeq 2000 paired-end sequencing. For effect of BRD4 bromodomain inhibitor (BRD4i), hSAECs were mock or RSV infected with or without ZL0454 (10 μM) for 24 h [49]. The trimming software CutAdapt (v0.1) was used to process raw fastq files [50]and fastQC was used for QC statistics. The trimmed paired-end reads were aligned against human genome hg38 using Salmon (1.10.3.12). Mapped paired-end reads for both genes and transcripts (isoforms) were counted in each sample using transcripts per million (TPM). Hierarchical clustering (HC) was performed with pHeatMap package in R (version 1.0.12).

Western blot and co-immunoprecipitation

Two 100-mm dishes of confluent hSAEC were used (5.5×10^6 cells/plate) were used as mock controls, while the other two were infected with RSV (MOI 1, 16 h). Cells were dissociated using recombinant trypsin-like enzymes (TrypLE, Thermo) and washed three times with cold phosphate-buffered saline (PBS). The resulting pellets were resuspended in low-ionic strength buffer [50 mM NaCl, 0.1% IGEPAL, 10% glycerol, 10 mM HEPES (pH 7.4)] containing a protease inhibitor cocktail (Millipore #11873580001) and phenylmethanesulfonyl fluoride (PMSF) (Thermo #36978). Pellets from two dishes were pooled into 1 ml of buffer, pipetted thoroughly, and incubated on ice for 30 min.

The cell lysates were then sonicated twice and centrifuged at 10 000 × *g* for 10 min at 4°C. From each sample, 100 μl of supernatant was reserved as input and separate western blot analysis. The remaining 450 μl of supernatant per group was incubated overnight at 4°C with 1.34 μl of IgG antibody (LS-Bio, LS0C149375, 5 mg/ml) or 9 μl of BRD4 antibody (Cell Signaling #13 440, 748 μg/ml, 1:50 dilution) with rotation.

On the following day, 30 μl of protein G Dynabeads (Invitrogen #10-003-D) was added to each sample and incubated for 2 h at 4°C on a rotator. Beads were then washed twice with low-ionic strength buffer using a magnetic stand. To elute the proteins, 30 μl of 2 × sodium dodecyl sulfate–polyacrylamide gel electrophoresis sample buffer was added, and the samples were boiled at 95°C for 5 min.

The protein samples were resolved on a 4%–15% TGX gel (Bio-Rad #5671083) and transferred to a PVDF membrane (Bio-Rad #1704157) using the Bio-Rad Turbo Transfer system. The membranes were subsequently probed with an SMARCA4 antibody (Invitrogen MA5-31550) to detect the target protein.

Proximity ligation assay

Proximity ligation assay (PLA) was performed with Duolink *in situ* red starter mouse/rabbit kit (Sigma DUO92101). Cells were treated, fixed with 4% paraformaldehyde, permeabilized with 0.1% Triton X-100, and incubated overnight with indicated pairwise combinations of rabbit IRF1 (Proteintech 11335-1-AP, 1:200), mouse SMARCA4 (Invitrogen MA5-31550, 1:500) for IRF1–SMARCA4, and mouse SMARCA4, rabbit BRD4 (Cell signaling 13440, 1:500) for SMARCA4–BRD4. The nuclei were counterstained with DAPI, and the PLA signals were visualized with an ECHO fluorescent microscope at ×20 magnification.

Chromatin immunoprecipitation

To capture indirect protein–protein interactions interacting with target chromatin, two-step chromatin immunoprecipitation (XChIP) was conducted. In brief, 3100 mm dishes of cells each treatment group were first cross-linked with disuccinimidyl glutarate (2 mM, 45 min at 22°C, Thermo 20593), then cross-linked with methanol-free formaldehyde (1% vol/vol in PBS, 10 min). Cells were extracted in sodium dodecyl sulfate lysis buffer and sonicated. Equal amounts of sheared chromatin were immunoprecipitated overnight at 4°C with 3 μg of antibody (Ab). To capture proteins directly interacting with target chromatin, single step cross-linking was performed using 1% formaldehyde. The following antibodies were used in immunoprecipitation (IP): IRF1 (Proteintech 11335–1-AP), BRD4 (Cell Signaling 13 440) and SMARCA4 (Proteintech, 11335–1-AP); IgG was a nonspecific binding control (LS Bio LS-C149375). IPs were collected with 30 μl of Dynabeads protein G (Thermo 10004D), washed, eluted and decrosslinked. The precipitated DNA was phenol/chloroform-extracted, precipitated and air-dried. Gene enrichment was determined by quantitative genomic PCR (Q-gPCR) using promoter-specific PCR primers (Supplementary Table S2). The fold change of precipitated DNA was determined by normalizing to input DNA and calculating the fold change relative to the amount in unstimulated cells [51, 52].

CUT&RUN

WT or SMARCA4 KD hSAECs were mock or RSV infected (MOI = 1.0, 24 h) in biological triplicates. Cells were trypsinized, quantitated, and 4×10^6 cells were incubated on ice for 10 min in 1 ml of nuclear extraction buffer [20 mM HEPES (pH 7.9), 10 mM KCl, 0.1% Triton X-100, 20% glycerol, 1× cOmplete proteinase inhibitor, 1x protein phosphatase inhibitor cocktail, 0.5 mM spermidine], the released nuclei were pelleted at 600 × *g*, 5 min at 4°C. The nutated nuclei were resuspended in antibody buffer produced by diluting 5 μg of anti-SMARCA4 Ab in 500 μl of Triton X-100-free wash buffer [WB; 20 mM HEPES (pH7.5), 150 mM NaCl, 0.05% Triton X-100, 0.1% bovine serum albumin (BSA), 1× cOmplete proteinase inhibitor, 1× protein phosphatase inhibitor cocktail, 0.5 mM spermidine], and incubated with nutation overnight at 4°C. The nuclei were washed and incubated at 4°C for 1 h in 50 μl of WB containing 2.5 μl of EpiCypher pAG-MNase 20× stock (EpiCypher, NC). Chromatin cleavage was conducted by incubating the nuclei on ice for 1 h in 150 μl of BSA-free WB containing 2 mM $CaCl_2$. The

cleavage was terminated by adding 150 µl of stop buffer [300 mM NaCl, 20 mM ethylenediaminetetraacetic acid, 4 mM EGTA, 0.5 ng of *Escherichia coli* spike-in DNA (EpiCypher, NC) per 150 µl]. The samples nutated at 4°C for 1 h, centrifuged at 16 000 × *g* for 5 min at 4°C and the supernatant was collected. The DNA fragments were phenol-chloroform extracted, glycogen precipitated, and dissolved in 20 µl of 0.1× TE buffer. CUT&RUN DNA libraries were prepared using NEBNext Ultra II DNA Library Prep Kit for Illumina (NEB, MA) per the manufacturer's instruction, with modification in SPRI bead clearance of adaptor ligation and library amplification reactions to retain small-sized DNA fragments. The quality of the resultant DNA libraries was confirmed by Agilent TapeStation HS DNA assay (Agilent, Santa Clara, CA, USA), and paired-end Illumina next generation sequencing (NGS) was carried out on NovaSeq 6000 with 5 million reads per sample.

Fastqc files were analyzed for quality metrics (Phred score, GC content, and duplication) using fastQC. Adapters were trimmed using TrimGalore. Genome alignment was by MACS2 to the GRCh38.p13 (hg38) genome assembly (NCBI) [53]. Peak calling was using SEACR with top 20% peaks cutoff [54]. Differential peak occupancy was determined using DIFFBIND v4.2 using DESEQ2 [55]. Super enhancer analysis was using HOMER v4.11 [56]. Metadata analysis was using Genomic Regions Enrichment of Annotations Tool (GREAT) [57]; genome ontology was using the reactome knowledge base [58]. Visualization of chromosomal coverage of peaks was performed using ChIPseeker [59]. Cleavage patterns were visualized using the Integrative Genomics Viewer (IGV) [60].

Assay for transposase-accessible chromatin sequencing

Assay for transposase-accessible chromatin sequencing (ATAC-seq) hSAEC cells were performed in two biological replicates per treatment [61]. Alignment was performed using RSubread package (v3.11) to the GRCh38.p13 (hg38) genome assembly (NCBI). Peak calling was performed using Genrich for ATAC-seq, using commands to remove mitochondrial sequences, remove PCR duplicate reads and mask blacklisted sequences. Statistical analysis was performed using DESEQ2 in the DiffBind package (v2.16.0), accepting an adjusted *P*-value of <.05 as significant.

Statistical analyses

RNA-seq was quantitated from Illumina High Seq fastq files. The raw fastq files were subjected to QC statistics and sequencing adapters were trimmed using Trim Galore software [62]. The trimmed paired-end reads were aligned against human genome hg38 using Salmon [63]. Mapped paired-end reads for both genes and transcripts (isoforms) were counted in each sample and variance stabilized using DESeq2 [33]. Statistical analyses were performed with Graph Pad Prism 9 (GraphPad Software, San Diego, CA). Results are expressed as mean ± SD. Normality and equal variance tests were performed to determine appropriate application of parametric statistical analyses. For multiple group experiments, one-way ANOVA was used with *post-hoc* Tukey T-tests for group-wise comparison between treatments. *P*-values <.05 were considered to be statistically significant.

Results

SMARCA4 primes the intrinsic IIR

We investigated the role of SMARCA4 in coupling of intrinsic immunity with cellular plasticity in a well-characterized small airway-derived basal cell expressing TP63 and KRT5 progenitor markers [13, 64]. hSAECs undergo partial mesenchymal transition in response to viral replication [11], Toll-like receptor (TLR) [65], and transforming growth factor beta (TGFβ) stimulation [66], activating metabolic reprogramming and extracellular matrix remodeling characteristic of basal cells *in vivo* [11, 13]. Finally, hSAECs differentiate into specialized ciliated, club and mucus-secreting goblet cells in air liquid interfaces, making these cells a valid airway basal cell model [15].

Building on our earlier finding that SMARCA4 regulates inflammatory gene expression, we determined the effect of SMARCA4 KD on the intrinsic IIR. RNA-seq profiles of a time course of RSV-infected hSAECs expressing nontargeting or SMARCA4-directed small hairpin (sh)RNA that reduce the BAF complex to 20% of WT cells [13] were extracted and the *Z*-scored gene expression profiles of 383 inflammatory response genes were examined by HC. The major patterns of gene expression segmented into four patterns (Fig. 1A). A small cluster of genes had high levels of basal expression and were reduced by RSV infection (Cluster I; Fig. 1A), whereas other clusters were increased by RSV infection (Clusters II, III, and IV; Fig. 1A). Within the RSV-increased profile, Cluster II included genes whose peak level of expression were at 16 h after infection, falling by 24 h, whereas Clusters III and IV were genes that peaked 24 h and later. We noticed the expression profiles of the rapidly responding genes in Cluster II were substantially reduced in the SMARCA4 KD cells (Fig. 1A). Inspecting the genes within this cluster, we noted that the core genes of the IRF1-regulated intrinsic immune response pathway were substantially enriched.

The intrinsic IIR is a core antiviral pathway under IRF1 feed-forward control that mediates antiviral response to RSV replication [14, 15]. The genes within this pathway include bone marrow stromal cell antigen 2 (BST2), interferon-induced protein with tetratricopeptide repeats (IFIT1), and IFN lambda (IFNL). Demonstrated by our earlier studies, evidence that these genes are directly regulated by IRF1 has been shown by four criteria: (i) ectopic IRF1 expression enhances expression of each messenger RNA (mRNA); (ii) IRF1 KD reduces their basal and viral-inducible expression; (iii) IRF1 binds directly to their core promoters; and (iv) IRF1 binding is required for activated polymerase recruitment and gene expression [15]. Interestingly, IRF1 expression *itself* is autoregulated, potentiated by IFN signaling providing a mechanism for amplification of intrinsic antiviral signals. To better visualize the impact of SMARCA4 KD on the IRF1-regulated intrinsic immune response, an HC was performed on the intrinsic subgroup (Fig. 1B). Here, we noted that these genes were uniformly highly expressed within 16 h of infection, and substantially inhibited in the SMARCA4 KD cells.

To provide quantitative information on the effect of SMARCA4 KD on the intrinsic IIR pathway, gene expression patterns were independently quantitated by qRT-PCR. First, efficiency of KD was confirmed, where we observed that cells expressing SMARCA4-directed shRNA had *SMARCA4* mRNA transcript abundance of 20 ± 3% of that of nontargeted shRNA controls in either the mock or RSV-infected state ($n = 4$, $P < .001$; Fig. 1C). We observed that expression of core

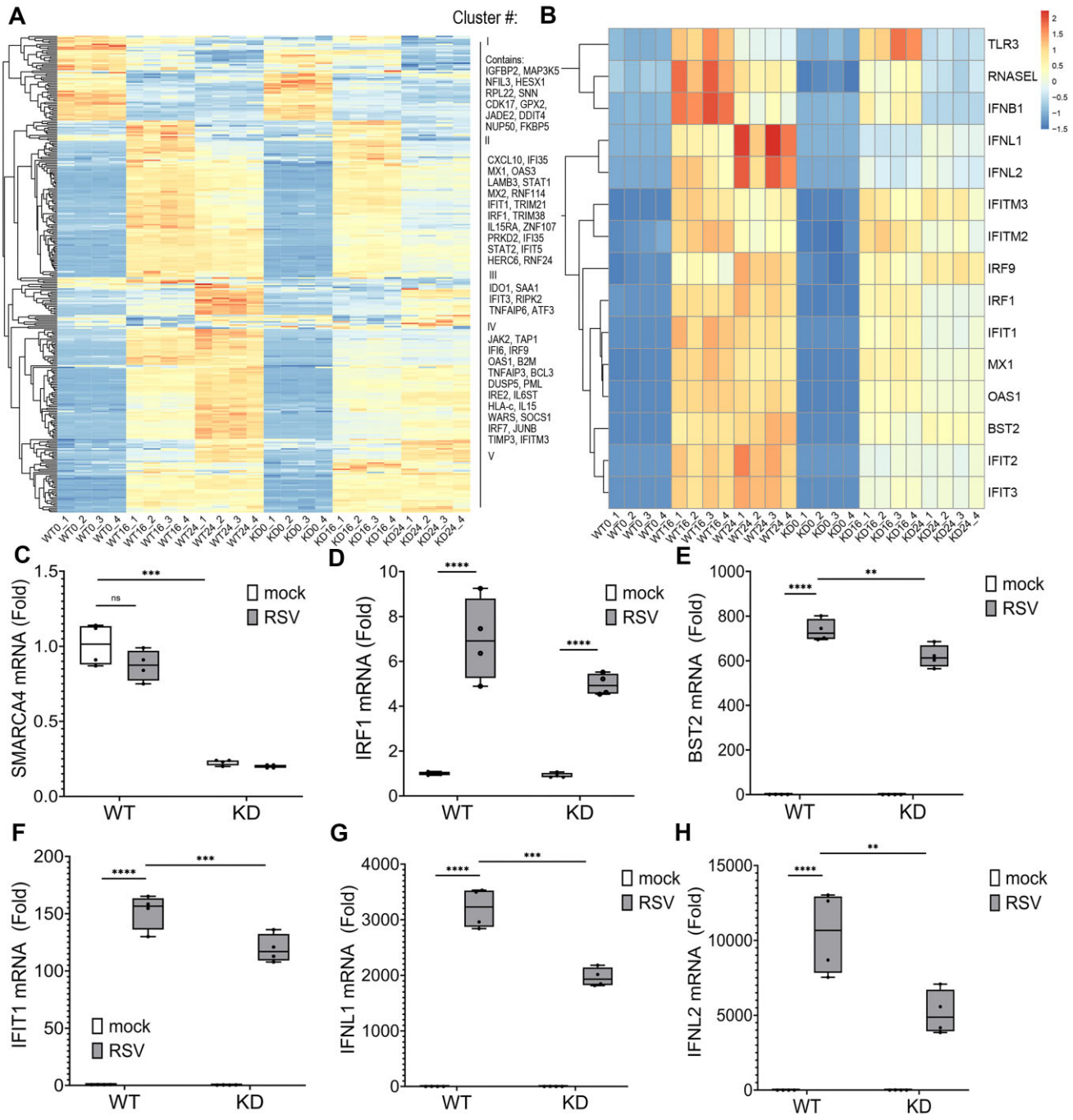

Figure 1. SMARCA4 is required for activation of the IRF1-dependent intrinsic IIR. (**A**) Shown is HC of mRNA expression of 298 ISGs in control shRNA (WT) or SMARCA4-targeted shRNA (SMARCA4 KD) hSAECs infected with RSV for 0 (mock), 16, or 24 h. RNA-seq data are *Z*-scored across the row. At right, representative genes in each subcluster are listed. (**B**) HC of IRF1-dependent intrinsic IIRs. Each row represents a gene, labeled at right. (C, D) Quantitation of intrinsic immune pathway genes in RSV-infected WT or SMARCA4 KD cells by qRT-PCR. For each gene, fold change in mRNA is shown. (**C**) SMARCA4, (**D**) IRF1 mRNA, (**E**) BST2 mRNA, (**F**) IFIT1 mRNA, (**G**) IFNL1 mRNA, and (**H**) IFNL2 mRNA. Each symbol is an independent biological replicate ($n = 4$). *, $P < .05$; **, $P < .01$; ***, $P < .001$; ****, $P < .0001$; ANOVA with *post-hoc*.

genes within the RSV-induced intrinsic IIR were consistently reduced in SMARCA4 KD cells (Fig. 1D–H). Specifically, RSV induced *BST2* mRNA 736 ± 50-fold in WT cells and this activation was reduced to 620 ± 50-fold in the SMARCA4 KD cells ($n = 4$, $P < .01$; Fig. 1E). Similarly, the 152-fold induction of *IFIT1* mRNA was reduced to 120-fold in KDs ($n = 4$, $P < .001$; Fig. 1F); the 3207-fold induction of *IFNL1* was reduced to 1970-fold in KDs ($n = 4$, $P < .001$; Fig. 1G); and the 10 500-fold induction of *IFNL2* was reduced to 1970-fold in KDs ($n = 4$, $P < .001$; Fig. 1H). Collectively we concluded that SMARCA4 is required for optimal induction of the IRF1-driven core of intrinsic IIR genes.

IRF1 dynamically complexes with SMARCA4

In ChIP experiments, we found that IRF1 was directly constitutively engaged with SMARCA4 on the proximal promoters of the core intrinsic IIR genes, priming them for rapid acti-

vation by viral replication through a transcriptional elongation mechanism involving formation of phosphorylated RNA polymerase II (RNA Pol II), recruiting BRD4 [15]. To better understand this mechanism, we sought to understand the effects of RSV on steady state abundances of these proteins. For this purpose, we examined a time course of RSV-induced IRF1 protein accumulation in western blot. Here, we observed that RSV induced a 2.5-fold increase in IRF1 protein abundance at 8 and 16 h, returning to that of mock-infected cells after 24 h (Fig. 2A). A similar two-fold burst of rapid induction was also observed for SMARCA4 and BRD4 proteins (Fig. 2B).

Previous affinity-mass spectrometry studies have found that IRF1 binds to the SMARCA4 complex in cells [67]. To confirm this association in hSAECs and avoid artifacts from cellular disruption, we applied an independent protein interaction assay using PLAs. PLAs detect atomic-distance interactions *in situ* detected by the enzymatic ligation of separately directed antibody-conjugated oligonucleotides that are amplified by PCR, appearing as red foci in immunofluorescence [68]. We observed that IRF1 was engaged with SMARCA4 in the nuclei of mock-infected cells (Fig. 2C), and this association was significantly increased 2.8-fold after RSV infection (Fig. 2D) as measured by the number of counts/nuclei ($P < .0001$, $n = 200$ nuclei; Fig. 2E).

To determine whether SMARCA4 binds to IRF1-dependent genes, ChIP experiments were performed. Here, cross-linked chromatin from mock or RSV-infected WT hSAECs were immunoprecipitated with nonspecific IgG or SMARCA4 Abs, and the abundance of the *BST2*, *IFITM1*, and *TLR3* proximal promoters were quantitated by Q-gPCR. We first estimated the binding of SMARCA4 in mock (uninfected) cells, where gene enrichment from SMARCA4 immunoprecipitates was estimated relative to background IgG binding. In uninfected hSAECs, we observed a 4.2-fold enrichment of SMARCA4 binding to the *BST2* promoter over IgG background by Q-gPCR ($n = 3$, $P < .01$; Fig. 2F). Similarly, we found a 6-fold enrichment in constitutive IRF1 binding on the *IFITM1* promoter over IgG background ($n = 3$, $P < .01$; Fig. 2G) and an 8.7-fold increase of IRF1 was observed on the *TLR3* promoter ($n = 3$, $P < .01$ Fig. 2H). By contrast, comparing SMARCA4 abundance in RSV-infected versus uninfected cells, the pseudo-steady state abundance of SMARCA4 was not substantially increased, with only *IFITM1* binding being statistically significant (Fig. 2F–H). These data indicate SMARCA4 is engaged with intrinsic IIR genes in resting cells and has variable degrees of recruitment in the setting of RSV infection.

BRD4 is required for RSV-induced epithelial mesenchymal plasticity

Our previous work discovered that BRD4 functions as an inducible coactivator with SMARCA4 in activation of ISGs, a gene network represented in Clusters III and IV (Fig. 1A), downstream of the intrinsic IIR [69]. To determine whether BRD4 was functionally required for coupled intrinsic innate IIR and epithelial plasticity, we explored the cellular effects of a highly selective BRD4i—ZL0454 [49]. ZL0454 is a cell-permeable, high affinity competitive inhibitor of both BRD4 acetyl lysine binding bromodomains (BD)-1 and -2 with an affinity of ~30 nM [48, 70]. To explore its effect on epithelial plasticity, we took advantage of the information that differentiated hSAECs form intercellular TJs containing epithelial cadherin (CDH1+) whose degradation is the hallmark, first committed state of cellular plasticity [71, 72]. To determine if BRD4 is functionally required for RSV-induced cellular plasticity, hSAECs were mock or RSV infected in the absence or presence of BRD4 and stained for CDH1 by immunofluorescence microscopy. In mock-infected hSAECs, we observed a uniform intercellular CDH1 staining pattern, indicating the presence of an extensive network of intercellular TJs (Fig. 3A, top left). In response to RSV infection, hSAECs showed a dramatic change in morphology as well as substantial dissolution of the TJs with internalization of CDH1 (Fig. 3A, top right). By contrast, mock-infected BRD4i-treated cells showed increased TJs, and retained TJs after RSV infection (Fig. 3A, bottom right). These findings demonstrate the essential involvement of BRD4 in RSV-induced cellular plasticity.

RSV induces SMARCA4–BRD4 association

Building on its central role in coupling SMARCA4 with intrinsic IIR and cellular plasticity, we next investigated whether RSV induces SMARCA4–BRD4 interactions using PLAs in mock or RSV-infected cells. In contrast to its interaction with IRF1, we observed that SMARCA4 had very low-to-undetectable interaction with BRD4 in mock-infected cells (Fig. 3B). In striking contrast, RSV replication induced a significant 14.3×10^3-fold induction of nuclear SMARCA4–BRD4 complexes ($P < .0001$, $n = 200$ nuclei; Fig. 3B and C). To independently confirm SMARCA4–BRD4 interaction, we performed nondenaturing co-immunoprecipitation (Co-IP) of RSV-infected cellular extracts. Immune complexes from IgG anti-BRD4 Co-IPs were fractionated and SMARCA4 detected. We observed a striking enrichment of SMARCA4 in the BRD4 immune complexes (Fig. 3D). These data confirm that SMARCA4 complexes with BRD4 in RSV-infected hSAECs.

BRD4 activity cooperates with SMARCA4 in RSV-induced innate responses

Remarkably, we also found that all of the intrinsic innate response genes induced by RSV were substantially inhibited by BRD4i treatment (Fig. 3E). Examination of the effect of BRD4i on expression of IRF1 and core genes of the intrinsic IIR also demonstrated a robust inhibition (Fig. 3F). For comparison with the effects of SMARCA4 KD, individual expression profiles were analyzed. Here, IRF1 mRNA increased three-fold in response to RSV infection, an increase that was substantially reduced by BRD4i treatment (Fig. 3D). Similarly, RSV-induced mRNA expression of *BST2*, *IFIT1*, *IFNL1*, and *TLR3* were all reduced by BRD4i treatment ($n = 3$, Fig. 3H–K). Collectively these data indicate that cooperation between SMARCA4 and BRD4 mediates induction of the core IRF1-responsive genes.

SMARCA4 coordinates RSV-BRD4 genomic positioning

These data indicate that SMARCA4–BRD4 mediate RSV-induced intrinsic IIR coupled to cellular plasticity. We therefore hypothesized that SMARCA4 coordinated BRD4 recruitment at the genomic level. To test this question, we analyzed BRD4 binding distribution in WT and SMARCA4 KD cells using an optimized chromatin immuno-cleavage/CUT&RUN—next-generation sequencing assay [21, 46]. Here, isolated nuclei from control or RSV-infected WT and SMARCA4 KD

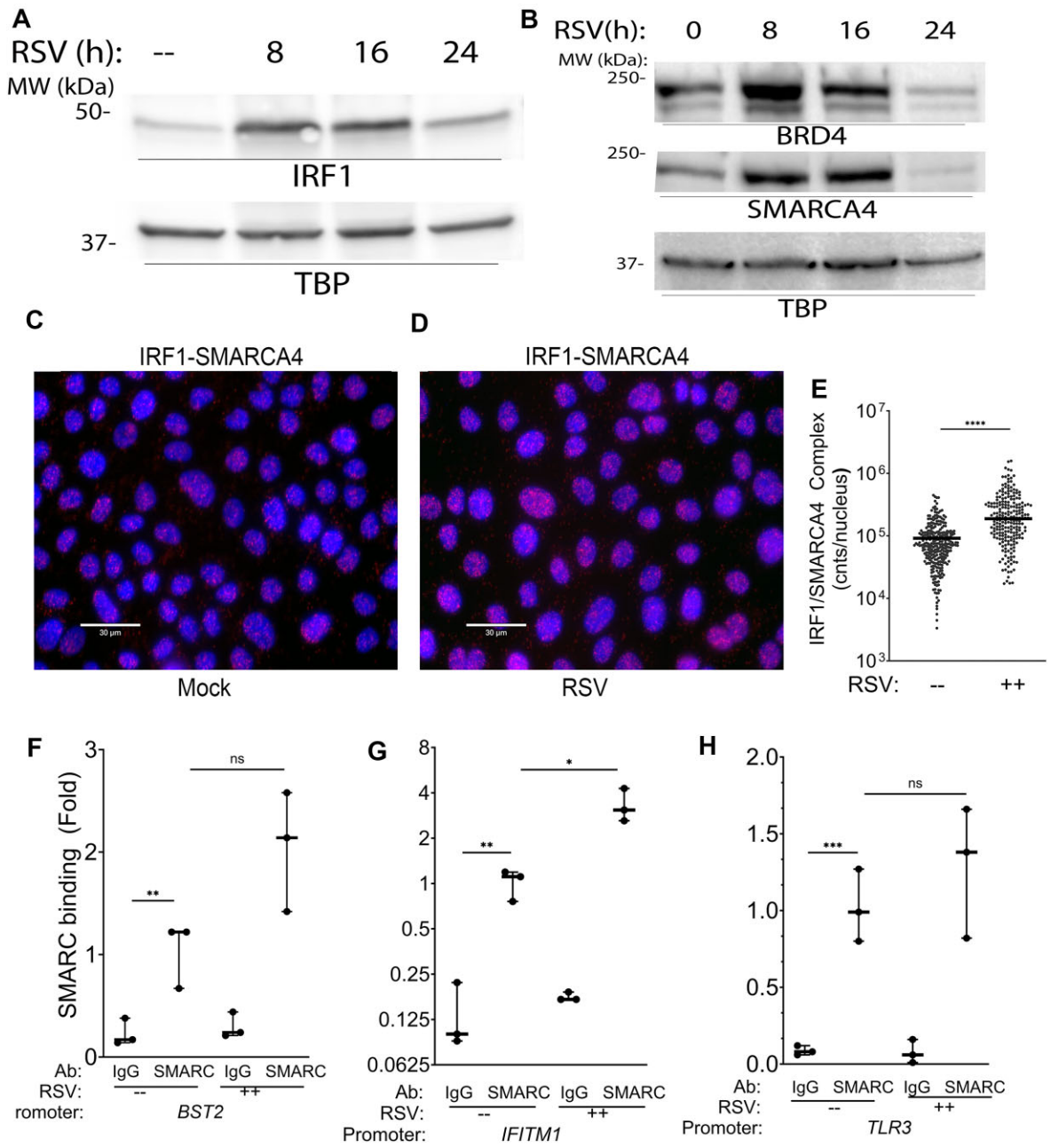

Figure 2. IRF1 engages SMARCA4 on intrinsic promoters. Western immunoblot of hSAECs in response to a time course of RSV infection (MOI = 1) for mock, 8, 16, or 24 h as indicated. (**A**) IRF1 protein with TBP as reference. TBP, TATA Box protein; MW, molecular weight (kDa). (**B**) Western for BRD4 and SMARCA4 proteins. PLAs were performed with rabbit anti-IRF1 and mouse anti-SMARCA4 Abs on mock (**C**) or RSV-infected hSAECs (**D**) (MOI = 1; 24 h). After secondary antibody reaction and PCR amplification, regions of interaction are indicated by dots. Nuclei are counterstained with DAPI. Scale marker is 30 μM. (**E**) Quantitation of IRF1–SMARCA4 nuclear complexes. PLAs from panels (C) and (D) were quantitated from >200 nuclei in >5 independent fields. Each symbol represents a complex from >200 nuclei. ****, $P < .0001$. XChIP of SMARCA4 binding to BST2 (**F**), IFITM1 (**G**), and TLR3 (**H**) proximal promoters. Shown are fold enrichment by Q-gPCR relative to IgG. Note the enrichment of SMARCA4 binding in mock-infected cells (–) over IgG for all promoters. ***, $P < .001$; ****, $P < .0001$; n.s., not significant.

hSAECs were incubated with validated BRD4 Ab, and regions of binding were released using protein A–protein G-micrococcal nuclease (pAG-MNase). Released fragments are then ligated to adapters, subjected to NGS and sequencing reads were subjected to quality assessment. The libraries produced high-confidence base calling of >150 bp with Phred scores >30 (not shown). After trimming, CUT&RUN generated fragment sizes from BRD4 Ab were ~70–100 nt in length consistent with an internucleosomal fragment distribution (Supplementary Fig. S1). By contrast, control fragment sizes in the IgG precipitates were monotonically larger, consistent with a nonspecific cleavage pattern. The libraries were aligned to both the hg38 and the *E. coli*-spike in genomes. An alignment frequency of 86%–91% unique fragments to the hg38 genome was observed for all the treatment conditions, with 5%–12% alignment to the *E. coli* genome (Supplementary Fig. S2). Sequencing depth and scaling factors used in the analysis are shown in Supplementary Table S2.

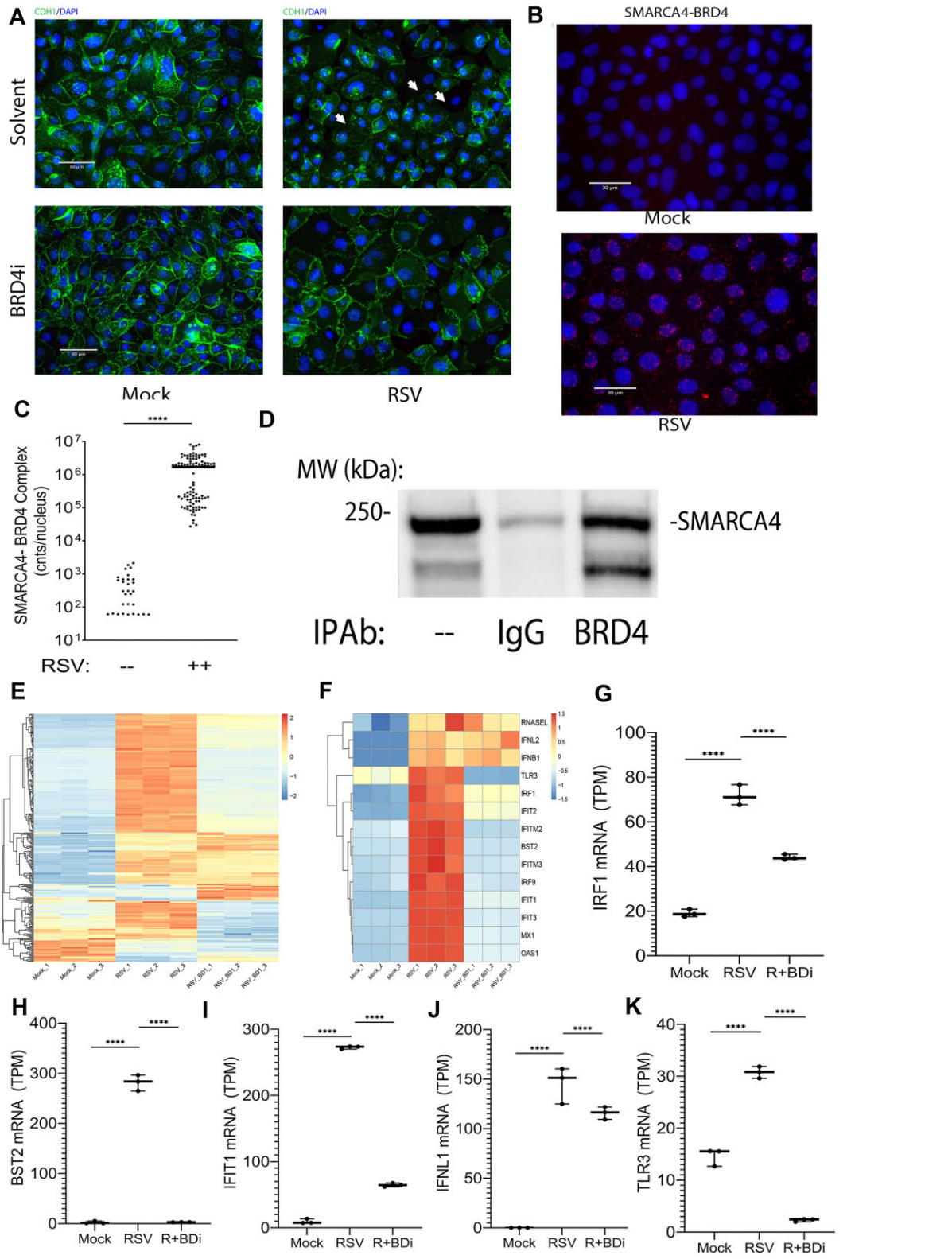

Figure 3. BRD4 associates with SMARCA4 and couples innate IIR to cellular plasticity. (**A**) Immunofluorescent staining of TJ formation in hSAECs. WT hSAECs were mock or RSV infected (MOI = 1; 24 h) in the presence of vehicle or ZL0454 (BRD4i). Cells were fixed and stained with CDH1 to visualize TJs and with DAPI to visualize nuclei. Scale bar in microns is shown. Arrows indicate loss of TJ boundaries in the RSV-infected cells. Note the relative preservation of TJs with BRD4i treatment. (**B**) PLA quantitation of SMARCA4–BRD4 interactions. Shown are fluorescence microscopy of mock (top panel) or RSV-infected hSAECS (bottom panel). (**C**) Quantitation of nuclear SMARCA4–BRD4 foci from >200 nuclei in >5 independent fields. Each symbol represents a complex from >200 nuclei. ****, $P < .0001$. (**D**) Co-IP of SMARCA4. RSV-infected cells were immunoprecipitated with IgG or anti-BRD4 Ab as indicated. Immune complexes were eluted and abundance of SMARCA4 detected by western. MW, molecular weight (kDa). Lane 1, input protein. (**E**) HC of mRNA expression (in log-stabilized TPM) of 298 ISGs for hSAECs in vehicle-treated hSAECs or BRD4i-treated hSAECs (ZL0454, 10 μM) in mock or RSV-infected. (**F**) HC of IRF1-dependent core genes. Quantitation of mRNA expression for IRF1 mRNA (**G**), BST2 (**H**), IFITM1 (**I**), IFNL1 (**J**), and TLR3 mRNAs (**K**). ***, $P < .001$; ****, $P < .0001$.

Examining sample similarity, we found that the DNA fragments co-clustered by immunoprecipitating antibody, genome, and treatment type (Fig. 4A), indicating this represented a high-quality and reproducible dataset.

We first analyzed BRD4 distribution in unstimulated hSAECs. After normalization to library depth and scaling for variations in spike-in efficiency, statistically significant peaks occupied by BRD4 relative to IgG were identified using DESEQ2 in DiffBind (the DESEQ2 $P_{adj} < .05$ was used as a cutoff to accommodate for multiple hypothesis testing). We identified enrichment of 4017 high-confidence, BRD4-occupied peaks versus nonspecific IgG background (Fig. 4B). To identify genes functionally regulated by BRD4-occupied regulatory regions, the differentially enriched peaks were subjected to analysis using GREAT [57], a tool that enhances identification of distal regulatory region by incorporating 3D conformation information to assign functional peaks to regulatory domains. Using this analysis, we noted that BRD4 bound regulatory genes include microcephalin 1 (MCPH1), Wnt family member 9a (WNT9A), TGFBR2, and X-box binding protein 1 (XBP1) (Fig. 4B). MCPH1 mediates SMARCA4 recruitment [27] to relax chromatin enabling spreading of γH2AX spreading [73] during DNA damage repair. WNT9A and TGFBR2 provide signals to activate plasticity programs in epithelial mesenchymal transition, whereas XBP1 mediates the unfolded protein response necessary for restoring cellular homeostasis in mesenchymal transition and priming the IRF1 response [46]. The distribution of BRD4 peaks on target genes was next examined in meta-gene analysis. We noted that in mock-infected cells, BRD4 peaks were distributed 50–500 kb downstream of the transcription start sites (TSSs), within gene bodies (Fig. 4C). To better understand the role of these BRD4-engaged domains in cellular processes, enrichment for biological processes (BioPs) was conducted in GREAT, where we found that the most highly statistically significant enrichments of BRD4-interacting genes were those controlling cell motility, survival, and proliferation (Fig. 4D).

We next examined the distribution of BRD4 peaks within highly enriched genes relative to transcriptionally active regulatory regions using IGV [74]. Examining the BRD4-dependent innate response gene, *IFNL2*, we observed two major BRD4 peaks spanning exons 3 and 4 that were within active chromatin (indicated by Ac-H3K27 peaks), and open, NFRs, as determined by enhanced cleavage in ATAC-seq [13], indicated by the arrowheads (Fig. 4E). In a manner consistent with the meta-gene analysis, a much smaller BRD4 peak was observed over the *IFNL2* promoter, which was in a closed chromatin domain (*, Fig. 4E, top panel). A similar finding was observed for the highly enriched BRD4 binding domain on *WNT9A* (arrowhead, Fig. 4E, bottom panel). From these data, we conclude that BRD4 is engaged on a subset of innate immunity and cellular plasticity genes.

RSV redistributes BRD4 to regulate stress and plasticity programs

Previous ATAC-seq studies showed that RSV induces global reorganization of inducible enhancers within epithelial cells [46]. To address how RSV controls BRD4 targeting during activation of the intrinsic innate response, CUT&RUN peaks were compared between uninfected versus RSV-infected WT cells. RSV produced significant changes in 2339 BRD4 peaks (using DESEQ2 to accommodate for multiple hypothesis-testing). Here, the global correlation between mock- and RSV-infected cells was less distinct than that between BRD4 and IgG Abs (c.f. Fig. 4A), reflective of the fact that RSV repositions count only ∼50% all BRD4 binding regions in the genome (Fig. 5A). RSV induces both gain and loss of BRD4 binding peaks, with 1354 peaks increasing and 985 peaks being reduced in BRD4 abundance (Fig. 5B). We noted that RSV induces a high-level of BRD4 binding to the FAM110C (family with sequence similarity 110 member C) gene, an alpha tubulin-binding protein involved in cell motility. Similar increases in BRD4 peaks TP63, a characteristic marker of damage-associated epithelial progenitors mediating the injury response.

We also noted that BRD4 binding shifts to regulatory regions −500 to −50 kb upstream of the known TSSs (Fig. 5C). In RSV-infected cell, BRD4 associated BioPs identified are similarly affected, with highly significant regulation of oxidative stress, immune processes, and pathways emerging as highly significant (Fig. 5D). A metagene analysis of BRD4 binding in the RSV-inducible BRD4 peaks is shown in Supplementary Fig. S3, and effect of RSV on BRD4 peak distributions across chromosomes are in Supplementary Fig. S4.

The relationship among RSV-regulated BRD4 peaks, transcriptionally active chromatin (Ac-H3K27), and NFRs in the presence or absence of RSV infection for the innate response gene *OAS3* and *ISG15* were next visualized in IGV. Here, RSV induced an increase in BRD4 binding over the proximal promoter of *OAS3*—this region corresponded to a transcriptionally active chromatin domain and was within a NFR (arrowhead, Fig. 5E, left panel). Similarly, RSV induced increased BRD4 loading in a transcriptionally active region on the *ISG15* promoter (Fig. 5E, right panel). Collectively these findings suggest BRD4 is dynamically repositioned by RSV to activate intrinsic immunity, cell plasticity, metabolic shifts, cell proliferation, and acquisition of migratory properties.

RSV redistributes BRD4 "super enhancers" controlling proliferation and plasticity

Super enhancers are enhancer domains spanning MB lengths enriched in BRD4, cell-specific transcription factors, mediator complexes, and H3K27Ac marks that determine cell-type specificity genes [75]. To better understand super enhancer distribution in RSV-infected progenitor cells, normalized tag counts were calculated over 12.5 MB domains using Homer "findPeaks" [56]. Using criteria of "superEnhancer slope" of >1, 50 new super enhancers were identified (Fig. 6A), that mapped to regulatory regions −500 to −50 kb upstream and gene bodies (Fig. 6B). The most highly significant BioPs were regulation of immune response, cell–cell adhesion, and protein phosphorylation (Fig. 6C). However, we noted a number of super enhancers were associated with noncoding RNAs, including *NEAT1*, *LINC02353*, and *MIR4425* whose functions are not fully annotated.

We noted that RSV induced a super enhancer on an AcH3K27-rich, NFR on the gene body of pterin-4 alpha-carbinolamine dehydratase 2 (PCBD2; Fig. 6D). PCBD2 is a DNA-templated protein that promotes HNF dimerization and transcriptional activation [76]. The BRD4 super enhancer on PCBD2 is located within a large intron, and is substantially enriched by RSV infection (arrowhead, Fig. 6D).

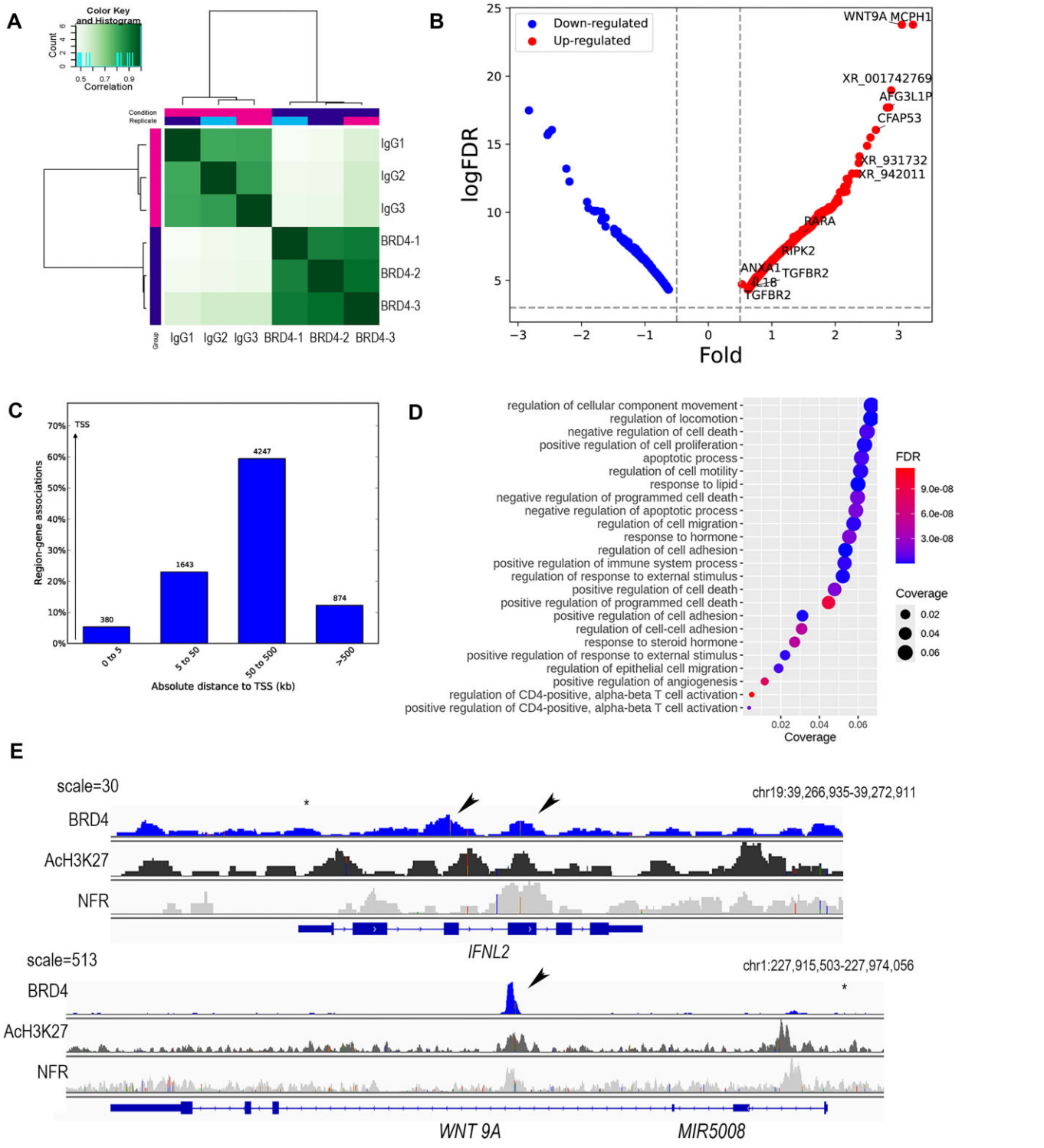

Figure 4. BRD4 genomic distribution in resting hSAECs. (**A**) Correlation plots of CUT&RUN fragments. Each individual replicate from uninfected (mock) cells immunoprecipitated with control IgG or BRD4 antibody were subjected to correlation analysis. Note the high cross-correlation of BRD4-immunoprecipitated fragments with each other that are distinct from those of control. (**B**) Volcano plot of BRD4 Ab enriched peaks in uninfected versus IgG. Differential analysis was determined after normalization to library depth and differential analysis using DiffBind. *X*-axis, fold change of binding occupancy; *Y*-axis, $-\log_{10}$(Benjamini–Hochberg-adjusted *P*-value, P_{adj}). Abbreviations: AG3L1P, AFG3-like matrix AAA peptidase; CFAP53, cilia and flagella-associated protein 53; TGFBR2 gene, TGFβ receptor 2; ANXA1 gene, annexin A1; RARA gene, retinoic acid receptor alpha; RIPK2, receptor interacting serine/threonine kinase 2. (**C**) Distribution of BRD4-containing peaks relative to gene bodies. Shown is a histogram of BRD4 peaks on gene bodies. Note the high frequency of BRD4 binding to proximal promoter sequences. (**D**) BioP enrichment. BioPs of genes with BRD4 binding to regulatory regions were identified and plotted. For each BioP, the fraction of genes represented in the pathway (coverage) and the adjusted *P*-value (P_{adj}) for the top 20 overrepresented pathways from GREAT-predicted genes are shown. Legend shows circle diameter of pathway coverage; color indicates significance of enrichment by fase discovery rate (FDR). (**E**) IGV of BRD4 peaks on *IFNL2* (top panel) and *WNT9A* (bottom panel) in mock-infected WT hSAECs. For each gene, BRD4 CUT&RUN tags are displayed along with acetylated H3K27 (AcH3K27) CUT&RUN peaks and nucleosome-free regions (NFRs) identified by ATAC-seq from mock-infected hSAECs. Note the distribution of BRD4 lies within AcH3K27 peaks in NFRs.

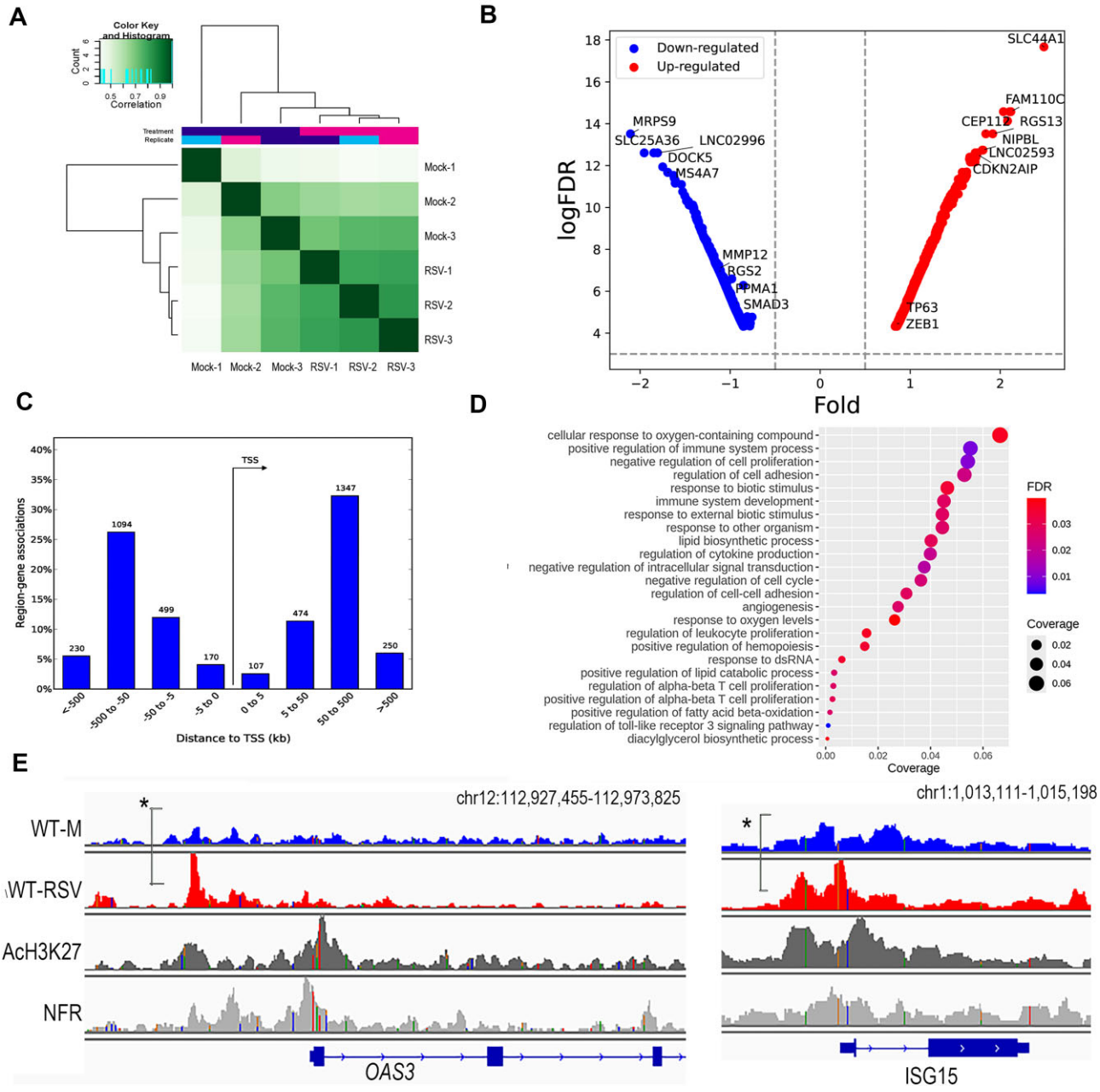

Figure 5. RSV repositions BRD4 to upstream promoters. (**A**) Correlation plots of CUT&RUN fragments. Individual replicates from uninfected (mock) and RSV-infected cells immunoprecipitated with BRD4 Ab were subjected to correlation analysis. (**B**) Volcano plot of BRD4 Ab-enriched peaks in mock versus RSV-infected cells. Differential analysis was determined after normalization to library depth and differential analysis using DiffBind. *X*-axis, fold change of binding occupancy; *Y*-axis, $-\log_{10}$(Benjamini–Hochberg-adjusted *P*-value, P_{adj}). Abbreviations: SLC44A1, solute carrier family 44 member 1; RGS13, regulator of G protein signaling 13; NIPBL, NIPBL cohesin loading factor; CDKN2AIP, CDKN2A interacting protein. (**C**) Distribution of BRD4-containing peaks relative to gene bodies. Shown is a histogram of BRD4 peaks on gene bodies. (**D**) BioP enrichment. For the top 20 overrepresented pathways, the fraction of genes represented in the pathway (coverage) and the adjusted *P*-value (P_{adj}) of genes mapped by GREAT are shown. Legend shows circle diameter of pathway coverage; color indicates significance of enrichment (FDR). (**E**) Left panel, IGV of BRD4 peaks on *OAS3* in WT hSAECs in the absence (M, mock) or presence of RSV infection (RSV). Right panel, IGV views of the *ISG15* promoter in WT hSAECs. For both panels, BRD4 CUT&RUN tags are displayed along with AcH3K27 CUT&RUN peaks and NFRs from ATAC-seq. Note the difference in BRD4 loading over the proximal OAS3 and ISG15 promoters (*) in RSV-infected versus mock-infected cells.

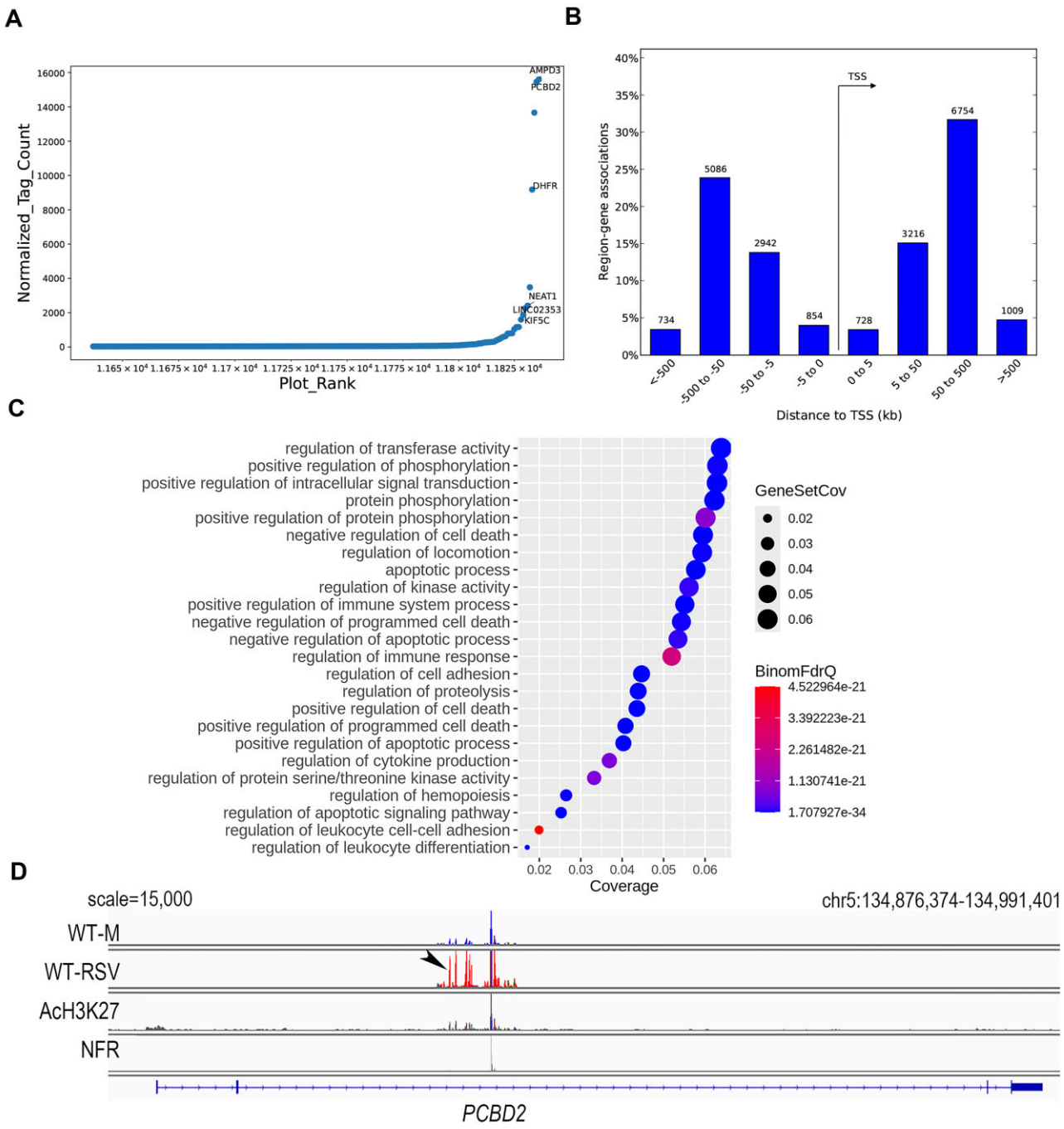

Figure 6. RSV repositions BRD4 binding in super enhancers. (**A**) Normalized tag counts were calculated for BRD4-enriched peaks in RSV-infected versus mock WT cells. Shown is a scatter plot of normalized tag count by rank order. Super enhancer peaks within genes are labeled. Abbreviations: AMPD3, adenosine monophosphate deaminase 3; DHFR, dihydrofolate reductase; LINCO02353, long intergenic nonprotein coding RNA 2353; K65C, kinesin family member 5C. (**B**) Distribution of BRD4-containing super enhancers relative to gene bodies. (**C**) The top 20 overrepresented BioPs are shown. (**D**) IGV of the *PCBD2* super enhancer within the intron. Note the increase in BRD4 loading in response to RSV infection (arrowhead).

SMARCA4 mediates BRD4 repositioning on a subgroup of peaks including intrinsic innate genes

Having established the pattern of constitutive and inducible BRD4 peaks in WT cells, we next sought to the role of SMARCA4 in BRD4 distribution by comparing BRD4 binding patterns in WT versus SMARCA4 KD. In a manner consistent with the low level of SMARCA4–BRD4 complexes in mock-infected cells (Fig. 2), there were no significant changes in BRD4 peaks in mock-infected WT versus mock-infected SMARCA4KD cells.

By contrast, 739 RSV-induced BRD4 peaks were affected by SMARCA4 KD (Fig. 7A); the majority of these were reduced (Fig. 7B). One of the most significantly changed SMARCA4-dependent BRD4 peak was collectin subfamily member 10 (COLEC10; Fig. 7B). COLEC10 is a C-lectin that binds to collagen important in cell adhesion, triggering endoplasmic reticulum (ER) stress and innate responses by binding carbohydrate sequences on invasive cytosolic microorganisms [77].

Mapping SMARCA4-dependent BRD4 peaks to genes, we noted that SMARCA4 sensitive BRD4 peaks were equally

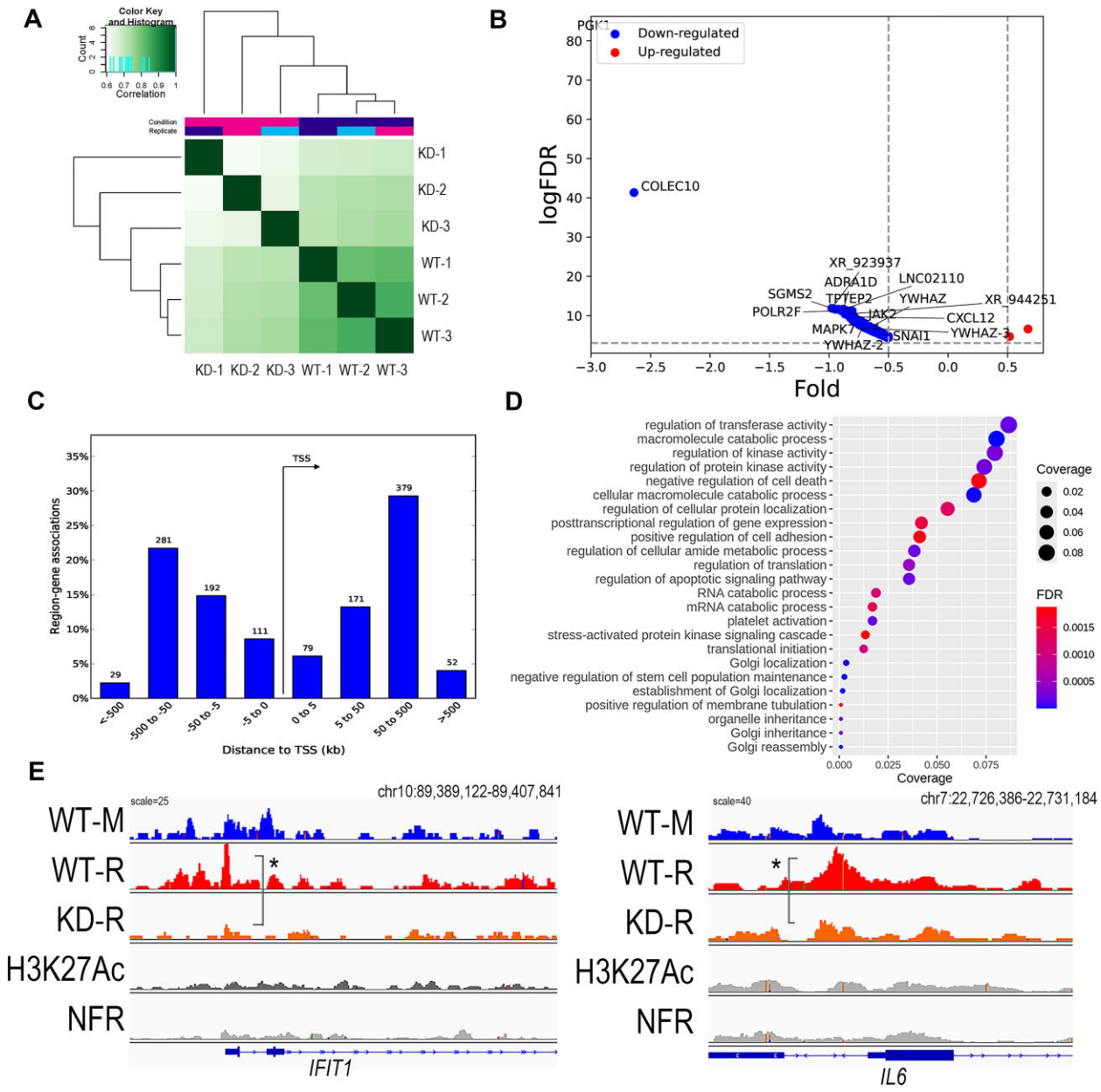

Figure 7. SMARCA4 mediates RSV-induced BRD4 repositioning. (**A**) Correlation plots of individual replicates from RSV-infected WT versus RSV-infected SMARCA4 KD cells. (**B**) Volcano plot of BRD4 Ab-enriched peaks in RSV-infected versus SMARCA4 KD cells. *X*-axis, fold change of binding occupancy; *Y*-axis, $-\log_{10}$(Benjamini–Hochberg-adjusted *P*-value, P_{adj}). Abbreviations: ADRA1D, adrenoceptor alpha 1D; POLR2F, RNA polymerase II, I, and III subunit F; YWHAZ, tyrosine 3-monooxygenase/tryptophan 5-monooxygenase activation protein zeta; MAPK, mitogen activated protein kinase. (**C**) Distribution of BRD4-containing peaks relative to gene bodies. (**D**) The top 20 overrepresented BioPs are shown. (**E**) Left panel, IGV of BRD4 peaks of *IFIT1* in WT and SMARCA4 KD in the absence (M, mock) or presence of RSV infection (RSV). Right panel, IGV of BRD4 peaks on the *IL6* promoter. BRD4 CUT&RUN tags are displayed along with AcH3K27 CUT&RUN peaks and NFR ATAC-seq from mock-infected hSAECs. Note the accumulation of BRD4 binding on the *BST2* promoter in response to RSV infection in WT cells (arrowhead), and its reduction in the SMARCA4 KD cells (*).

distributed over upstream regulatory elements and downstream gene bodies (Fig. 7C). A meta analysis showing the distinct regions of BRD4 binding affected by SMARCA4 KD is shown in Supplementary Fig. S3. The BioPs most highly affected by SMARCA4-dependent BRD4 peaks were post-transcriptional regulatory factors (kinases), cell adhesion, and RNA metabolism (Fig. 7D). Illustration of the differences in RSV-induced BRD4 peak distributions in WT versus KD cells across chromosomes are in Supplementary Fig. S5.

The distribution of SMARCA4-dependent BRD4 peaks relative to activated chromatin domains and NFRs on the innate response gene *IFIT1* was visualized in IGV. Here, we observed that RSV-induced accumulation of BRD4 peaks over the *IFIT1* promoter in transcriptionally active and open chromatin domains (Fig. 7E, left panel). Importantly, BRD4 promoter accumulation was markedly attenuated in the SMARCA4 KD cells (Fig. 7E, left panel, brackets). A similar induction of BRD4 peaks over the *IL6* promoter was observed in WT cells; this induction was markedly reduced in

the SMARCA4 KD cells (Fig. 7E, right panel). These findings provide direct mechanistic evidence that SMARCA4 regulates BRD4 recruitment to coordinate intrinsic immunity and epithelial plasticity.

SMARCA4 expands the boundaries of BRD4 super enhancers controlling cell motility

SMARCA4 KD reduced BRD4 abundance on 30 RSV-induced super enhancers distributed both upstream of the TSS and throughout gene bodies (Fig. 8A and B). The most significant BioPs regulated by SMARCA4-dependent BRD4 super enhancers were those controlling cellular locomotion, adhesion, cell stress, and protein kinase activity (Fig. 8C).

We visualized the SMARCA4-dependent BRD4 super enhancer on the receptor tyrosine kinase like orphan receptor 2 (ROR2). We noted RSV-induced BRD4 binding to the *ROR2* super enhancer within the second intron in WT cells, and this reduction was substantially reduced in the SMARCA4 KDs (arrowhead, Fig. 8D and zoomed image). Interestingly to us, upon closer examination, we noted that the NFRs were extended in both the 3′ and 5′ direction beyond the BRD4 domains in the RSV-infected WT cells [compare NFR in WT–mock versus WT–RSV (Supplementary Fig. S6)]. This expansion of NFR region was not observed in the RSV-infected SMARCA4 KD cells. We observed a similar phenomenon on the BRD4 super enhancer on the 3′ UTR of *COLEC10* (Supplementary Fig. S6). In the absence of SMARCA4, BRD4 binding to the *COLEC10* super enhancer was completely ablated. A similar pattern of inducible expansion of the NFR was seen in the RSV-infected WT cells that was absent with the RSV-infected SMARCA4 KD cells. Discussed below, these data suggest that SMARCA4 participates in RSV-induced chromatin dynamics in the super enhancer complex.

SMARCA4-dependent BRD4 binding regulates lncRNAs controlling intrinsic immunity autocrine loops

In our analysis, we noted SMARCA4-regulated BRD4 peaks correspond to noncoding RNAs that regulate intrinsic immunity, providing novel insights into how SMARCA4 activity may affect intrinsic IIR. In particular, ISR8/IRF1-AS/colitis-associated IRF1 antisense regulator of intestinal homeostasis is a nuclear lncRNA on human chromosome 5 oriented in a head-to-tail configuration downstream of the IRF1 gene that enhances IRF1 expression [78–80]. We found an SMARCA4-dependent BRD4 peak spanning the IRF1 locus with local enrichment on a NFR region over the *ISR8* promoter that was enriched in transcriptionally active H3K27Ac marks (Fig. 9A). In response to RSV infection, BRD4 binding is enhanced over *ISR8*; this binding abundance was dramatically reduced by SMARCA4 KD (Fig. 9A). Additionally, a BRD4-containing peak binds the IRF1 enhancer/promoter (epromoter, IRF1^{Enh}), also located within a NFR and enriched in H3K27Ac marks (Fig. 9B). We previously showed the *IRF1*^{Enh} functionally mediates inducible *IRF1* mRNA expression in RSV infected cells by targeting a KRAB-repressor to this region [21]. Like that over the *ISR8* promoter, RSV-induced BRD4 binding to the *IRF1*^{Enh} was also reduced by SMARCA4 KD (Fig. 9B).

To further understand this mechanism, we confirmed that SMARCA4 directly binds *ISR8* in ChIP. Relative to nonspecific IgG, SMARCA4 Ab enriched *ISR8* promoter 1.8 ± 0.5-fold in mock-infected cells, and further increased to 4.5 ± 0.4-fold after RSV infection ($P < .01$; Fig. 9C). Confirming the patterns seen in CUT&RUN, BRD4 binding to *ISR8* promoter in ChIP was enriched 5.6 ± 1.2-fold binding over that of IgG in mock-infected cells that further increased 14.3 ± 3.9-fold after RSV infection ($P = .011$; Fig. 9D).

A similar pattern of SMARCA4 binding was observed on the *IRF1*^{Enh}, with 3.6 ± 0.8-fold enrichment in mock-infected cells that increased to 7.7 ± 1.5-fold after RSV infection ($P = .012$; Fig. 9E). Similarly, BRD4 binding to the *IRF1*^{Enh} was 11 ± 1-fold enriched over IgG in mock-infected cells that was further increased 74 ± 6.4-fold after RSV infection ($P < .001$; Fig. 9F). These findings confirm the patterns of BRD4 binding in the CUT&RUN studies and extend them to demonstrate SMARCA4 is directly binding to these key regulatory domains on the IRF1 locus.

To examine whether BRD4 binding was required for IRF1 enhancer activity, the effect of a BRD4i (ZL0454) on RSV-inducible *ISR8* lncRNA expression was tested [48]. We observed that BRD4i reduced *ISR8* lncRNA abundance by five-fold in mock infected cells. The 10.6 ± 0.8-fold increase in *ISR8* lncRNA was reduced to 3.6 ± 0.6 in the presence of BRD4i ($P = .002$; Fig. 9G). Similarly, the *IRF1*^{Enh} promoter expresses a noncoding RNA; BRD4i reduced both mock and RSV-induced IRF1^{Enh} lncRNA by four-fold relative to vehicle treatment ($P < .01$; Fig. 9G). These data indicate that SMARCA4 controls intrinsic immunity, in part, through recruiting functional BRD4 to the I*RF1* locus by affecting regulatory noncoding RNA expression.

Discussion

Persistent activation of mucosal injury and repair is a common pathogenic mechanism of chronic obstructive airway diseases responsible for substantial morbidity, mortality, and economic impact. In particular, lower respiratory tract infections with the ubiquitous human *orthopneumovirus*, RSV, produce epithelial death and barrier dysfunction activating coupled intrinsic immunity and cellular plasticity programs [10, 11]. In the developing lung, effects of severe RSV infection and its dyregulatory effects on basal cell differentiation [47] result in lifelong persistent reductions in lung function, enhanced utilization of health care resources, and an increased risk of premature respiratory fatality [38–41]. Understanding the mechanisms of how this infection triggers epithelial plasticity are therefore highly significant. Although RSV primarily replicates in terminally differentiated epithelial cells producing cell death and sloughing [42–44, 81], basal cells, by contrast, are relatively resistant to infection, enabling this population to serve a critical role in epithelial regeneration [82].

Our study advances the understanding of the epigenetics of innate injury-repair in multipotent lower airway basal epithelial cells [15]. Here, we use a model TP63+/KRT5 + basal cell capable of differentiating into club, ciliated, and goblet cells [15]. *In vivo*, TP63+/Krt5 + basal cells expand, migrate, and repopulate the injured lower airway in response to viral infection and oxidative damage, making this cell type central to injury-response [9, 18–20]. Viral injury to these cells activates a series of cell-state transitions mediated by induction of both EMT and MET regulators supported by shifts in intracellular metabolic pathways [11, 21]. Protection of this basal cell pop-

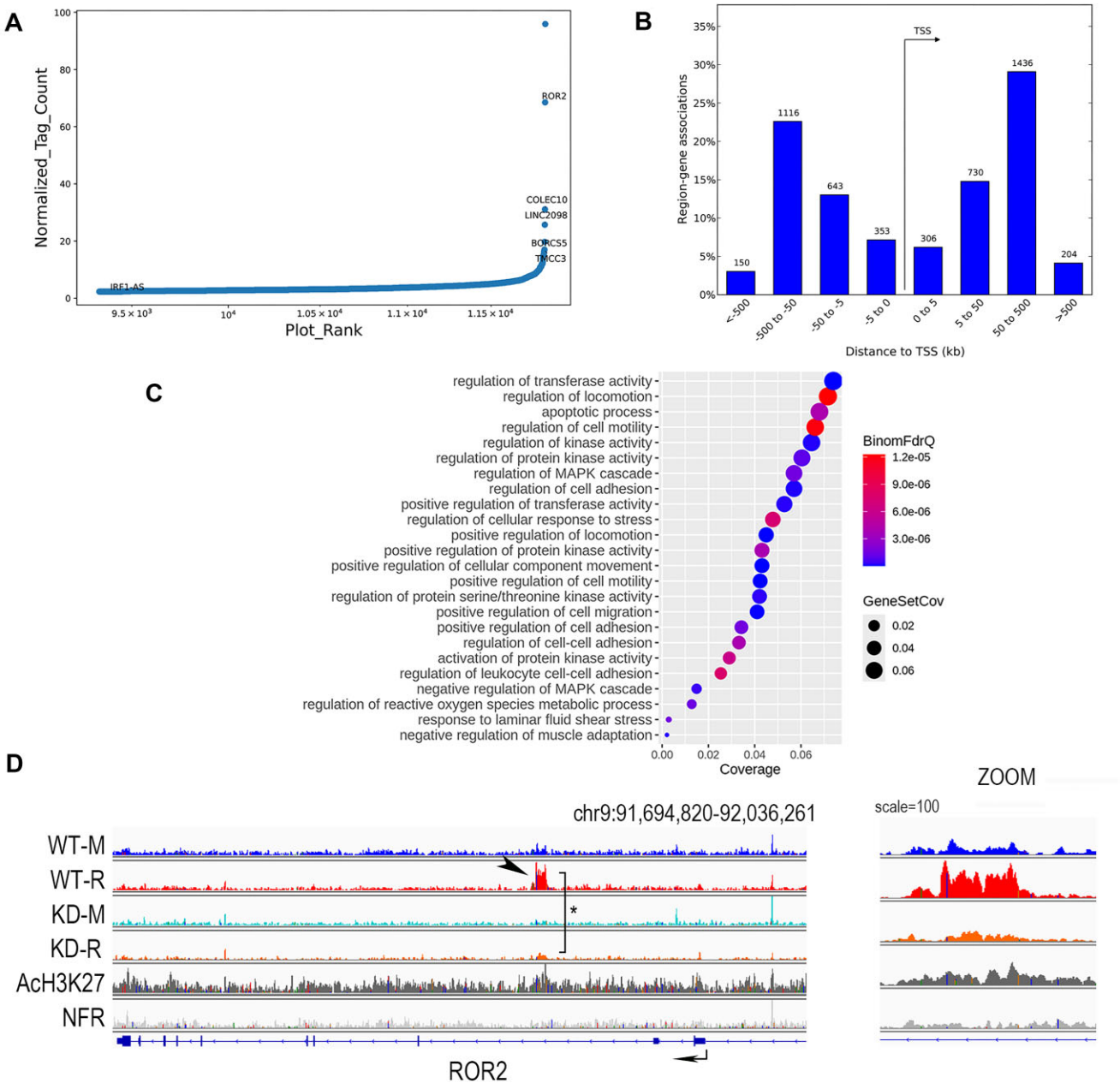

Figure 8. SMARCA4-dependent, RSV-induced BRD4 super enhancer formation. (**A**) Normalized tag counts of BRD4-enriched peaks in RSV-infected WT versus SMARCA4 KD cells. *X*-axis, rank order; *Y*-axis, norrmalized tag count. (**B**) Distribution of SMARCA4-dependent BRD4-containing super enhancers relative to gene bodies. Abbreviations: BORCS5, BLOC-1 related complex subunit 5; TMCC3 transmembrane and coiled-coil domain family 3. (**C**) The top 20 overrepresented BioPs are shown. (**D**) IGV of BRD4 super enhancers on *ROR2* in WT and SMARCA4 KD cells in the absence (M, mock) or presence of RSV infection (RSV). BRD4 CUT&RUN tags are displayed along with NFR ATAC-seq from mock-infected or RSV infected WT and SMARCA4 KD cells. Zoomed image is shown at right. Note the increase in super enhancer peaks in RSV infected versus mock infected WT cells (arrowhead) and reduction in the SMARCA4 KD cells (*).

ulation from viral infection is important for the regeneration of the epithelial surface. The IRF1 intrinsic innate response plays this important role.

Previous work has shown that these multipotent cells are inherently resistant to viral infections via the presence of the intrinsic IIR [14]. Here, constitutive expression of IRF1 directly activates a core of IFN-stimulated genes including *BST2*, *IFITM1*, *TLR3*, and others to produce constitutive viral resistance [15]. Interestingly, these genes are expressed in an IFN-independent manner where they function to antagonize viral replication at multiple stages of viral transcription, replication, and secretion [83]. We observe that intrinsic pathway is regulated in two modes by SMARCA4. In unstimulated conditions, IRF1 is engaged with SMARCA4, but in the setting of innate challenge, we find that BRD4 complexes with SMARCA4 required for high level induction of antiviral response. Strikingly SMARCA4 and BRD4 are not only key regulators of the intrinsic IIR, but also regulators of epithelial plasticity. Downregulation of SMARCA4 triggers unscheduled transition into EMT, whereas BRD4 is required for degradation of epithelial TJs, as well as expression of mesenchymal transcription factors.

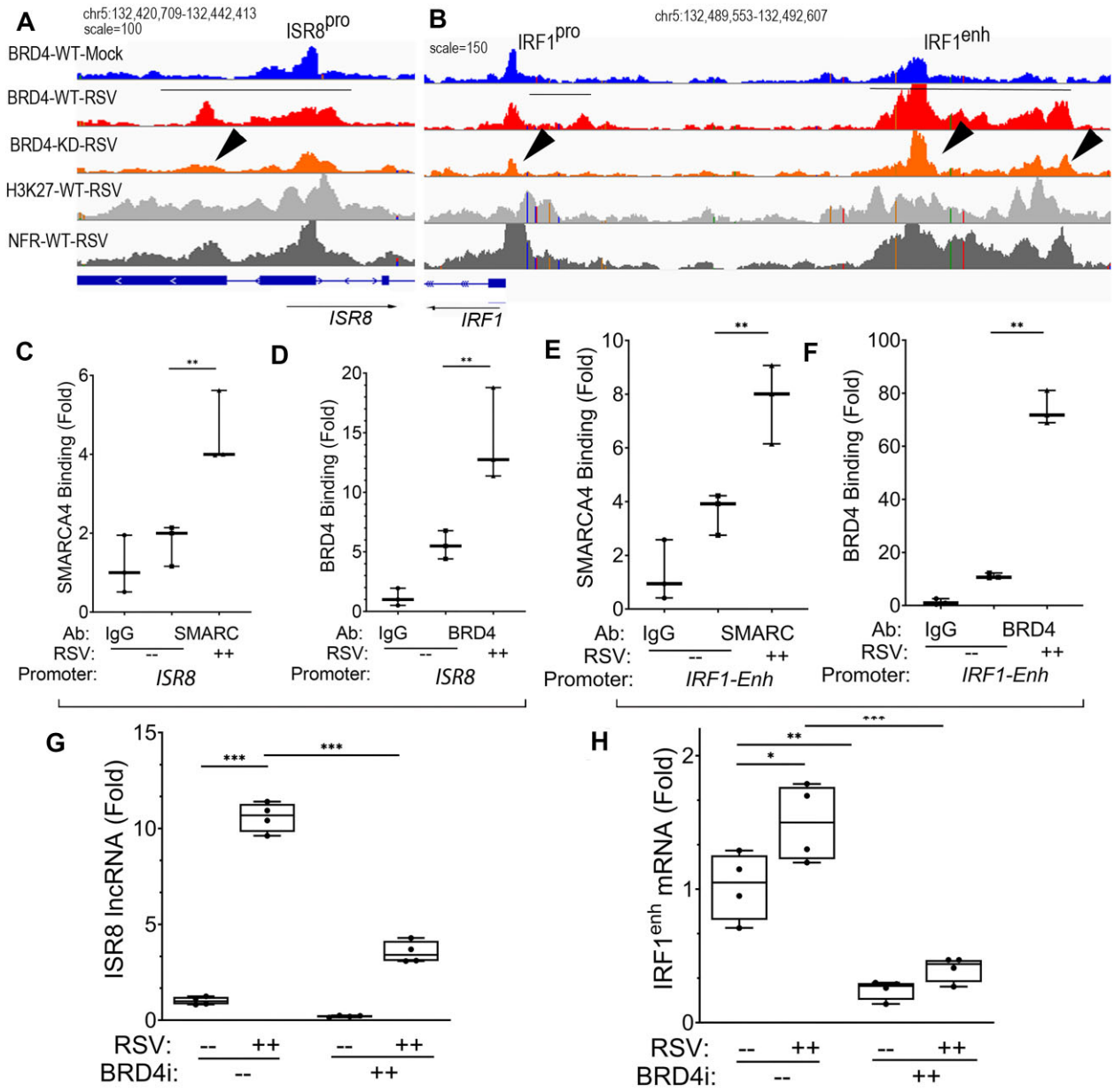

Figure 9. SMARCA4–BRD4 regulation of noncoding RNAs in intrinsic immunity. (**A**) IGV of BRD4 super enhancers on *ISR8* promoter in WT and SMARCA4 KD cells in the absence (M, mock) or presence of RSV infection (RSV). For each gene, BRD4 CUT&RUN tags are displayed along with NFR ATAC-seq and H3K27Ac peaks. Arrowheads indicate location of reduced BRD4 binding in SMARCA4 KD. (**B**) IGV of BRD4 super enhancers on the IRF1 epromoter ($IRF1^{Enh}$). (**C**) ChIP of SMARCA4 binding to *ISR8* promoter. Enrichment of ISR8 in hSAECs immunoprecipitated with IgG or SMARCA4. Shown are fold enrichment by Q-gPCR. (**D**) ChIP of BRD4 binding on *ISR8* promoter. (**E**) ChIP of SMARCA4 binding to $IRF1^{Enh;}$ treatment conditions are as in panel (C). (**F**) ChIP of BRD4 binding to $IRF1^{Enh.;}$ treatment conditions are as in panel (C). (G, H) Cells were treated with or without BRD4i (10 μM ZL0454) in absence or presence of RSV. Noncoding RNA was detected by qRT-PCR. (**G**) *ISR8* lncRNA expression. (**H**) $IRF1^{Enh}$ expression. ***, $P < .001$; ****, $P < .0001$.

Although innate IIR and plasticity have traditionally viewed as distinct cell responses, our genome-wide profiling studies clearly indicate that the intrinsic IIR is mechanistically coupled with cellular plasticity programs. Reasoning that SMARCA4 may modulate BRD4 genomic targeting, we conducted a comprehensive CUT&RUN analysis of BRD4 interactions in the presence and absence of SMARCA4. Interestingly, SMARCA4 and BRD4 are transiently induced by RSV infection in parallel with that of IRF1. However, these levels rapidly return to that of control at times when BRD4 is coordinating intrinsic IIR and cellular plasticity programs. Given that BRD4 peaks are reduced at some regions and increased at others at times when BRD4 abundance is similar to that of control, we interpret this complex regulation to mean that BRD4 is dynamically repositioned to upstream regulatory elements, including super enhancers, controlling cellular plasticity, adhesion molecules, and cytokine genes. Our data further indicate that BRD4 targeting is complex and multifactorial. Although SMARCA4 regulates a subset of BRD4 peaks, SMARCA4–BRD4 repositioning participates in intrinsic innate response genes, as well as the autoregulation of IRF1 facilitating activity of the IRF1 upstream enhancer including its

downstream *ISR8* lncRNA. These data illustrate novel roles of SMARCA4 in the coupled processes of intrinsic immunity and epithelial plasticity by coordinating BRD4 distribution across the genome.

SMARCA4 primes antiviral defense pathways in progenitor cells

Current studies of cell-intrinsic immunity have focused on IFN-inducible antiviral responses of differentiated cells. Recently, the presence of the intrinsic immune pathway has been identified, a pathway that provides constitutive antiviral activity to progenitor and multipotent cells that is IRF1-dependent, yet independent of IFN signaling [14, 83]. Previous work that has shown a role for SMARCA4 in "priming" inducible response of IFN stimulated genes, displacing nucleosomes from proximal promoter locations and permissive for recruitment of HATs [84]. We earlier extended this mechanism to show IRF1 is constitutively engaged with activated RNA Pol II [15] and here show that IRF1 is also engaged with SMARCA4 on the intrinsic core promoters.

Genome-wide ATAC-seq studies showed a central, effect of SMARC4 KD on global chromatin opening of genes regulated during viral replication [13]. Phenotypically, SMARCA4 KD cells entered unscheduled de-differentiation and mesenchymal transition, losing *adherens junctions* complexes, activating growth factor expression and remodeling extracellular matrix (ECM) [13]. Our findings in this study extend the role of SMARCA4 in positioning innate and mesenchymal transition genes for rapid transcription elongation by BRD4 recruitment.

The global effect of SMARCA4 on super enhancers and cell stress pathways suggests that SMARCA4 may regulate higher order chromatin organization. In this regard, a ChIP sequencing (ChIP-seq) and chromatin conformation study of SMARCA4 KD in MCF-10A mammary epithelial cells identified pleiotropic roles of SMARCA4 in super enhancer formation, telomere organization, and maintenance of transcriptional activation domain boundary strength [85]. In this study, a compartmentalization analysis found that SMARCA4 binding was significantly enriched in open A-type chromatin regions with active gene expression, consistent with our study's implications that SMARCA4 is involved in priming intrinsic and plasticity genes for expression. Whether BRD4 positioning was enriched on high-level expression domains was not reported. Nevertheless, this study provides confirmation of the relationship among SMARCA4, super enhancers, and active chromatin in epithelial cell types.

SMARCA4 participates in the dynamic BRD4 repositioning in antiviral defense

Our studies suggest that BRD4 plays a central role in coordinating the intrinsic IIR through a mechanism involving repositioning its binds from gene bodies in quiescent cells to 5′ regulatory sites upstream of TSS, regions enriched in transcriptionally active and NFR chromatin domains. This interpretation is consistent with other ChIP-seq studies finding that BRD4 is dynamically repositioned to super enhancers controlling stress response and cell-type specification genes [30] through BD-mediated interactions with acetylated H3 and H4 histones [31]. Real-time imaging has shown that BRD4 binds acetylated histones in a mobile phase, with a rapid "on and off" binding mode, affected by degree of histone acetylation and requiring both BDs [86]. However, this mechanism cannot fully explain BRD4's dynamic repositioning nor why it associates with innate inducible transcription factors.

One of the most studied innate transcription factors interacting with BRD4 is RELA/NFκB. In quiescent cells, RELA is complexed in the cytoplasm but undergoes stimulus-induced acetylation on Lys 310, a post-translational modification permitting binding to the BRD4 BDs [32, 87]. In activated endothelial and epithelial cells, Ac-Lys310 NFκB targets BRD4 to super enhancers controlling inflammatory cytokines and unfolded protein response pathways [32, 88]. Upon targeting to proximal, immediate-early genes, BRD4 mediates rapid transcriptional elongation, activating paused hypo-phosphorylated polymerase to enter rapid processive mode [32]. Our studies here suggest that SMARCA4 plays a similar role, by repositioning of BRD4 to a subgroup of intrinsic IIR and plasticity genes. Whether SMARCA4 is within the RelA–BRD4 complex, or whether these are distinct complexes is currently unknown. Nevertheless, these data indicate that multiple factors control BRD4 dynamic localization within the genome.

SMARCA4-mediated BRD4 repositioning couples antiviral defense with intrinsic immunity

Our work provides a map of the viral-induced BRD4 binding landscape in chromatin that mediate innate immunity and mesenchymal transition in progenitor cells undergoing injury-repair programs. The biological pathways we have identified extend our understanding for the role BRD4 plays in activating coordinated processes of cell plasticity, ER-stress, and DNA repair in response to viral infections. The coordinate activation of *WNT9A* and *TGFBR2* play important roles in activating a TGFβ autocrine response important in mucosal regeneration [36, 89]. DNA damage-repair pathways maintain cellular viability in oxidative injury and viral infections [90]. Our finding that BRD4 is engaged with *MCPH1* gene suggests a mechanism how BRD4 facilitates the DNA-damage response, as *MCPH1* required for SMARCA4 recruitment to double-stranded DNA break-repair complexes [27]. Similarly mitigating ER stress induced by growth factor stimulated activation of ECM plays an important role in sustaining cellular viability as progenitor cells enter cellular plasticity [91]. We note that BRD4 engagement of the XBP1 poises the basal cell to produce sustained activation of the unfolded protein response to restore cellular proteostasis. Interestingly, XBP1 is a factor that potentiating IRF1 synthesis through the $IRF1^{Enh}$ in viral infection [11, 46].

The BRD4 complex coordinate key regulatory steps in gene expression

We speculate on why SMARCA4 recruits BRD4 to cell stress and motility pathways. BRD4 is a pleiotropic protein most intensively studied as a regulator of transcriptional elongation, a highly regulated step in expression of intrinsic innate genes. Here, rapidly inducible genes are maintained in an open chromatin configuration associated with stalled, hypo-phosphorylated RNA Pol II. Gene activation is produced by a switch from "stalled" to a "processive" polymerase mode producing full length transcripts [92]. In this activation, BRD4 mediates transcriptional elongation by (i) binding the cyclin dependent kinase complex to cooperatively phosphorylate the RNA Pol II CTD [33, 93], (ii) recruiting activated RNA Pol

II subunits [15, 94], and (iii) acetylating histones within the core nucleosome, destabilizing their binding on gene bodies, further promoting RNA Pol II translocation [57]. Our earlier studies suggested that IRF1 and BRD4 cooperate to regulate the intrinsic core promoters by regulating pSer2 Pol II loading [15]. In fact, transcriptional elongation is the major mechanism for activation of immediate early genes in RSV infection [32, 95], as well as activation of mesenchymal gene program in basal cells [92].

However, this transcriptional elongation model may be too simplistic, based on the findings that BRD4 complex controls several additional steps in inducible gene expression. Our unbiased liquid chromatography (LC)-tandem mass spectrometry (MS/MS) studies of BRD4 protein interactions have identified that BRD4 dynamically interacts with coactivators of enhancer driven transcription, RNA binding proteins and ribososomal subunits that may also be active [96]. For example, we identified unanticipated roles of BRD4 in mRNA splicing [97], an important component of the innate response [98]. More work will need to be done to understand the multiple functions in transcription-coupled splicing, translation, and nuclear structure mediated by this dynamic complex.

In addition to its ability to modulate nucleosomal decondensation, SMARCA4 has been found in lncRNA-binding paraspeckle complexes [28]. Here, SMARCA4, NONO, SFPQ, and other paraspeckle proteins bind the NEAT1–2 lncRNA forming the structural components of "nuclear bodies" also implicated in regulating the inflammatory response [99]. More work will need to be done to understand the role of SMARCA4 RNA binding activities in the cell stress response.

SMARCA4 regulation of super enhancer boundaries

Our observations in IGV suggest that SMARCA4 may contribute to growth of BRD4-dependent super enhancers by affecting the width of NFRs (Supplementary Fig. S6). Others have found that SMARCA4 exhibits ATP-dependent chromatin relaxation activity, a phenomenon implicated in the repair of DNA double-stranded breaks, enabling spreading of γH2AX foci and its repair proteins [27]. We suggest that the RSV-induced expansion of BRD4 super enhancers may mechanistically be similar to chromatin relaxation seen with γH2AX spreading.

SMARCA4 BRD4 mediate critical lncRNA expression controlling intrinsic immunity

The intrinsic pathway maintains constitutive antiviral defense through an IFN-independent IRF1 expression affecting constitutive antiviral activity [83, 100]. The IRF1 locus is under a complex regulatory activity by lncRNAs whose expression enhance IRF1 expression. In particular, *ISR8* is a nuclear -encoded lncRNA whose transcription is required for optimal IRF1 expression [79]. Although it is known that the *ISR8* lncRNA has feed-forward enhancement effect on IRF1 mRNA expression, the mechanisms controlling *ISR8* expression are not known. We discover here that SMARCA4 contributes to a BRD4 super enhancer spanning the IRF1 locus, and that BRD4 facilitates inducible *ISR8* lnc and $IRF1^{Enh}$ epromoter activity. This work extends the pleiotropic mechanisms that BRD4 uses to control intrinsic IIR. The effects of noncoding RNAs in maintaining intrinsic immunity in basal cells will be topics of future studies.

Conclusions

The TP63 + basal epithelial cells play a critical role in repopulating the airway after barrier disruption. The mechanisms how injury or infection couples with activation of plasticity and innate protection of the airway basal cell are incompletely understood. Using a model lower airway basal cell, we have explored the interactions of IRF1, SMARCA4, and BRD4 in regulating cellular plasticity. We find that ambient IRF1 complexes with SMARCA4 on intrinsic innate IIR genes maintaining them in a 'primed' state for activation. Upon viral infection, a burst of IRF1/SMARCA4/BRD4 synthesis occurs, where SMARCA4 complexes with BRD4 and repositions its binding through the genome. We describe, for the first time, the landscape of dynamic SMARCA4–BRD4 interactions on homeostatic cellular plasticity and intrinsic immunity pathways. This coordinated BRD4 recruitment and its pleiotropic regulatory mechanisms enables coupling of cell stress pathways ensuring basal cell survival to repair mucosal surfaces.

Acknowledgements

The authors acknowledge the support of the UW Genomics Core for next-generation sequencing.

Author contributions: All authors have read and agreed to the published version of the manuscript. Xiaofang Xu (Conceptualization, Data curation, Methodology, Writing—original draft, Writing—review & editing) and Allan R. Brasier (Conceptualization, Data curation, Funding acquisition, Investigation, Methodology, Data visualization, Writing—original draft, Writing—review & editing)

Supplementary data

Supplementary data is available at NAR online.

Conflict of interest

The authors declare no conflict of interest.

Funding

This work was partially supported by NIH grants AI062885 (A.R.B.), NCATS UL1TR002373 (A.R.B.), and NIAID 1U01AI136994 (A.R.B.). The funders had no role in the design of the study; in the collection, analyses, or interpretation of data; in the writing of the manuscript; or in the decision to publish the results. Funding to pay the Open Access publication charges for this article was provided by NIH.

Data availability

The datasets presented in this study can be found in online repositories. The names of the repository/repositories and accession number(s) can be found below: https://www.ncbi.nlm.nih.gov/geo/query/acc.cgi?acc=GSE179353 and https://www.ncbi.nlm.nih.gov/geo/query/acc.cgi?acc=GSE161849.

References

1. Raby KL, Michaeloudes C, Tonkin J *et al.* Mechanisms of airway epithelial injury and abnormal repair in asthma and COPD. *Front Immunol* 2023;**14**:1201658. https://doi.org/10.3389/fimmu.2023.1201658

2. Brasier AR. Innate immunity, epithelial plasticity, and remodeling in asthma. *Adv Exp Med Biol* 2023;**1426**:265–85. https://doi.org/10.1007/978-3-031-32259-4_13
3. Hogg JC, Chu F, Utokaparch S *et al.* The nature of small-airway obstruction in chronic obstructive pulmonary disease. *N Engl J Med* 2004;**350**:2645–53. https://doi.org/10.1056/NEJMoa032158
4. Harvey B-G, Heguy A, Leopold PL *et al.* Modification of gene expression of the small airway epithelium in response to cigarette smoking. *J Mol Med* 2006;**85**:39–53. https://doi.org/10.1007/s00109-006-0103-z
5. Tian B, Yang J, Zhao Y *et al.* Central role of the NF-kappaB pathway in the *Scgb1a1*-expressing epithelium in mediating respiratory syncytial virus-induced airway inflammation. *J Virol* 2018;**92**:e00441-18. https://doi.org/10.1128/JVI.00441-18
6. Wu K, Kamimoto K, Zhang Y *et al.* Basal epithelial stem cells cross an alarmin checkpoint for postviral lung disease. *J Clin Invest* 2021;**131**:e149336. https://doi.org/10.1172/JCI149336
7. Boers E, Barrett M, Su JG *et al.* Global burden of chronic obstructive pulmonary disease through 2050. *JAMA Netw Open* 2023;**6**:e2346598. https://doi.org/10.1001/jamanetworkopen.2023.46598
8. Chen S, Kuhn M, Prettner K *et al.* The global economic burden of chronic obstructive pulmonary disease for 204 countries and territories in 2020-50: a health-augmented macroeconomic modelling study. *Lancet Glob Health* 2023;**11**:e1183-93. https://doi.org/10.1016/S2214-109X(23)00217-6
9. Warner SM, Hackett TL, Shaheen F *et al.* Transcription factor p63 regulates key genes and wound repair in human airway epithelial basal cells. *Am J Respir Cell Mol Biol* 2013;**49**:978–88. https://doi.org/10.1165/rcmb.2012-0447OC
10. Xu X, Qiao D, Mann M *et al.* Respiratory syncytial virus infection induces chromatin remodeling to activate growth factor and extracellular matrix secretion pathways. *Viruses* 2020;**12**:804. https://doi.org/10.3390/v12080804
11. Qiao D, Skibba M, Xu X *et al.* Paramyxovirus replication induces the hexosamine biosynthetic pathway and mesenchymal transition via the IRE1alpha-XBP1s arm of the unfolded protein response. *Am J Physiol-Lung Cell Mol Physiol* 2021;**321**:L576–94. https://doi.org/10.1152/ajplung.00127.2021
12. Brasier AR, Qiao D, Zhao Y. The hexosamine biosynthetic pathway links innate inflammation with epithelial–mesenchymal plasticity in airway remodeling. *Front Pharmacol* 2021;**12**:808735. https://doi.org/10.3389/fphar.2021.808735
13. Xu X, Qiao D, Dong C *et al.* The SWI/SNF-related, matrix associated, actin-dependent regulator of chromatin A4 core complex represses respiratory syncytial virus-induced syncytia formation and subepithelial myofibroblast transition. *Front Immunol* 2021;**12**:633654. https://doi.org/10.3389/fimmu.2021.633654
14. Wu X, Dao Thi VL, Huang Y *et al.* Intrinsic immunity shapes viral resistance of stem cells. *Cell* 2018;**172**:423–38. https://doi.org/10.1016/j.cell.2017.11.018
15. Xu X, Qiao D, Brasier AR. Cooperative interaction of interferon regulatory factor-1 and bromodomain-containing protein 4 on RNA polymerase activation for intrinsic innate immunity. *Front Immunol* 2024;**15**:1366235. https://doi.org/10.3389/fimmu.2024.1366235
16. Erjefalt JS, Erjefalt I, Sundler F *et al. In vivo* restitution of airway epithelium. *Cell Tissue Res* 1995;**281**:305–16. https://doi.org/10.1007/BF00583399
17. Avila PC. Plasticity of airway epithelial cells. *J Allergy Clin Immunol* 2011;**128**:1225–6. https://doi.org/10.1016/j.jaci.2011.10.006
18. Beppu AK, Zhao J, Yao C *et al.* Epithelial plasticity and innate immune activation promote lung tissue remodeling following respiratory viral infection. *Nat Commun* 2023;**14**:5814. https://doi.org/10.1038/s41467-023-41387-3
19. Zheng D, Limmon GV, Yin L *et al.* Regeneration of alveolar type I and II cells from Scgb1a1-expressing cells following severe pulmonary damage induced by bleomycin and influenza. *PLoS One* 2012;**7**:e48451. https://doi.org/10.1371/journal.pone.0048451
20. Zuo W, Zhang T, Wu DZ *et al.* p63(+)Krt5(+) distal airway stem cells are essential for lung regeneration. *Nature* 2015;**517**:616–20. https://doi.org/10.1038/nature13903
21. Qiao D, Skibba M, Xu X *et al.* Genomic targets of the IRE1–XBP1s pathway in mediating metabolic adaptation in epithelial plasticity. *Nucleic Acids Res* 2023;**51**:3650–70. https://doi.org/10.1093/nar/gkad077
22. Xu X, Qiao D, Pan L *et al.* RELA·8-oxoguanine DNA glycosylase1 is an epigenetic regulatory complex coordinating the hexosamine biosynthetic pathway in RSV infection. *Cells* 2022;**11**:2210. https://doi.org/10.3390/cells11142210
23. Rock JR, Randell SH, Hogan BLM. Airway basal stem cells: a perspective on their roles in epithelial homeostasis and remodeling. *Dis Model Mech* 2010;**3**:545–56.
24. Rubin AJ, Barajas BC, Furlan-Magaril M *et al.* Lineage-specific dynamic and pre-established enhancer-promoter contacts cooperate in terminal differentiation. *Nat Genet* 2017;**49**:1522–8. https://doi.org/10.1038/ng.3935
25. Panda D, Gjinaj E, Bachu M *et al.* IRF1 Maintains optimal constitutive expression of antiviral genes and regulates the early antiviral response. *Front Immunol* 2019;**10**:1019. https://doi.org/10.3389/fimmu.2019.01019
26. Wilson BG, Wang X, Shen X *et al.* Epigenetic antagonism between polycomb and SWI/SNF complexes during oncogenic transformation. *Cancer Cell* 2010;**18**:316–28. https://doi.org/10.1016/j.ccr.2010.09.006
27. Peng G, Yim EK, Dai H *et al.* BRIT1/MCPH1 links chromatin remodelling to DNA damage response. *Nat Cell Biol* 2009;**11**:865–72. https://doi.org/10.1038/ncb1895
28. Kawaguchi T, Tanigawa A, Naganuma T *et al.* SWI/SNF chromatin-remodeling complexes function in noncoding RNA-dependent assembly of nuclear bodies. *Proc Natl Acad Sci USA* 2015;**112**:4304–9. https://doi.org/10.1073/pnas.1423819112
29. Wang R, Li Q, Helfer CM *et al.* Bromodomain protein Brd4 associated with acetylated chromatin is important for maintenance of higher-order chromatin structure. *J Biol Chem* 2012;**287**:10738–52. https://doi.org/10.1074/jbc.M111.323493
30. Whyte WA, Orlando DA, Hnisz D *et al.* Master transcription factors and mediator establish super-enhancers at key cell identity genes. *Cell* 2013;**153**:307–19. https://doi.org/10.1016/j.cell.2013.03.035
31. Devaiah BN, Case-Borden C, Gegonne A *et al.* BRD4 is a histone acetyltransferase that evicts nucleosomes from chromatin. *Nat Struct Mol Biol* 2016;**23**:540–8. https://doi.org/10.1038/nsmb.3228
32. Brasier AR, Tian B, Jamaluddin M *et al.* RelA Ser276 phosphorylation-coupled Lys310 acetylation controls transcriptional elongation of inflammatory cytokines in respiratory syncytial virus infection. *J Virol* 2011;**85**:11752–69. https://doi.org/10.1128/JVI.05360-11
33. Yang J, Zhao Y, Kalita M *et al.* Systematic determination of human cyclin dependent kinase (CDK)-9 interactome identifies novel functions in RNA splicing mediated by the DEAD box (DDX)-5/17 RNA helicases. *Mol Cell Proteomics* 2015;**14**:2701–21. https://doi.org/10.1074/mcp.M115.049221
34. Brasier AR, Boldogh I. Targeting inducible epigenetic reprogramming pathways in chronic airway remodeling. *Drugs Context* 2019;**8**:2019-8-3. https://doi.org/10.7573/dic.2019-8-3
35. Chang H, Liu Y, Xue M *et al.* Synergistic action of master transcription factors controls epithelial-to-mesenchymal transition. *Nucleic Acids Res* 2016;**44**:2514–27. https://doi.org/10.1093/nar/gkw126

36. Tian B, Widen SG, Yang J *et al.* The NFkappaB subunit RELA is a master transcriptional regulator of the committed epithelial–mesenchymal transition in airway epithelial cells. *J Biol Chem* 2018;**293**:16528–45. https://doi.org/10.1074/jbc.RA118.003662
37. Tian B, Zhao Y, Sun H *et al.* BRD4 mediates NF-kappaB-dependent epithelial–mesenchymal transition and pulmonary fibrosis via transcriptional elongation. *Am J Physiol Lung Cell Mol Physiol* 2016;**311**:L1183–201. https://doi.org/10.1152/ajplung.00224.2016
38. Sigurs N, Aljassim F, Kjellman B *et al.* Asthma and allergy patterns over 18 years after severe RSV bronchiolitis in the first year of life. *Thorax* 2010;**65**:1045–52. https://doi.org/10.1136/thx.2009.121582
39. Fauroux B, Simoes EAF, Checchia PA *et al.* The burden and long-term respiratory morbidity associated with respiratory syncytial virus infection in early childhood. *Infect Dis Ther* 2017;**6**:173–97. https://doi.org/10.1007/s40121-017-0151-4
40. Allinson JP, Chaturvedi N, Wong A *et al.* Early childhood lower respiratory tract infection and premature adult death from respiratory disease in Great Britain: a national birth cohort study. *The Lancet* 2023;**401**:1183–93. https://doi.org/10.1016/S0140-6736(23)00131-9
41. Rosas-Salazar C, Chirkova T, Gebretsadik T *et al.* Respiratory syncytial virus infection during infancy and asthma during childhood in the USA (INSPIRE): a population-based, prospective birth cohort study. *The Lancet* 2023;**401**:1669–80. https://doi.org/10.1016/S0140-6736(23)00811-5
42. Ganesan S, Comstock AT, Sajjan US. Barrier function of airway tract epithelium. *Tissue Barriers* 2013;**1**:e24997. https://doi.org/10.4161/tisb.24997
43. Lambrecht BN, Hammad H. Allergens and the airway epithelium response: gateway to allergic sensitization. *J Allergy Clin Immunol* 2014;**134**:499–507. https://doi.org/10.1016/j.jaci.2014.06.036
44. Whitsett JA, Alenghat T. Respiratory epithelial cells orchestrate pulmonary innate immunity. *Nat Immunol* 2015;**16**:27–35. https://doi.org/10.1038/ni.3045
45. Zhao Y, Qiao D, Skibba M *et al.* The IRE1α-XBP1s arm of the unfolded protein response activates N-glycosylation to remodel the subepithelial basement membrane in paramyxovirus infection. *Int J Mol Sci* 2022;**23**:9000. https://doi.org/10.3390/ijms23169000
46. Qiao D, Xu X, Zhang Y *et al.* RSV replication modifies the XBP1s binding complex on the IRF1 upstream enhancer to potentiate the mucosal anti-viral response. *Front Immunol* 2023;**14**:1197356. https://doi.org/10.3389/fimmu.2023.1197356
47. Persson BD, Jaffe AB, Fearns R *et al.* Respiratory syncytial virus can infect basal cells and alter human airway epithelial differentiation. *PLoS One* 2014;**9**:e102368. https://doi.org/10.1371/journal.pone.0102368
48. Liu Z, Tian B, Chen H *et al.* Discovery of potent and selective BRD4 inhibitors capable of blocking TLR3-induced acute airway inflammation. *Eur J Med Chem* 2018;**151**:450–61. https://doi.org/10.1016/j.ejmech.2018.04.006
49. Xu X, Mann M, Qiao D *et al.* Bromodomain containing protein 4 (BRD4) regulates expression of its interacting coactivators in the innate response to respiratory syncytial virus. *Front Mol Biosci* 2021;**8**:728661. https://doi.org/10.3389/fmolb.2021.728661
50. Martin M. Cutadapt removes adapter sequences from high-throughput sequencing reads. *EMBnet J* 2011;**17**:3.
51. Nowak DE, Tian B, Brasier AR. Two-step cross-linking method for identification of NF-kappaB gene network by chromatin immunoprecipitation. *BioTechniques* 2005;**39**:715–25. https://doi.org/10.2144/000112014
52. Tian B, Yang J, Brasier AR. Two-step cross-linking for analysis of protein-chromatin interactions. *Methods Mol Biol* 2012;**809**:105–20. https://doi.org/10.1007/978-1-61779-376-9_7
53. Zhang Y, Liu T, Eeckhoute J *et al.* Model-based analysis of ChIP-seq (MACS). *Genome Biol* 2008;**9**:R137. https://doi.org/10.1186/gb-2008-9-9-r137
54. Meers MP, Tenenbaum D, Henikoff S. Peak calling by sparse enrichment analysis for CUT&RUN chromatin profiling. *Epigenetics Chromatin* 2019;**12**:42.
55. Ross-Innes CS, Stark R, Teschendorff AE *et al.* Differential oestrogen receptor binding is associated with clinical outcome in breast cancer. *Nature* 2012;**481**:389–93. https://doi.org/10.1038/nature10730
56. Heinz S, Benner C, Spann N *et al.* Simple combinations of lineage-determining transcription factors prime *cis*-regulatory elements required for macrophage and B cell identities. *Mol Cell* 2010;**38**:576–89. https://doi.org/10.1016/j.molcel.2010.05.004
57. McLean CY, Bristor D, Hiller M *et al.* GREAT improves functional interpretation of *cis*-regulatory regions. *Nat Biotechnol* 2010;**28**:495–501. https://doi.org/10.1038/nbt.1630
58. Milacic M, Beavers D, Conley P *et al.* The Reactome Pathway Knowledgebase 2024. *Nucleic Acids Res* 2024;**52**:D672–8. https://doi.org/10.1093/nar/gkad1025
59. Wang Q, Li M, Wu T *et al.* Exploring epigenomic datasets by ChIPseeker. *Current Protocols* 2022;**2**:e585. https://doi.org/10.1002/cpz1.585
60. Robinson JT, Thorvaldsdóttir H, Winckler W *et al.* Integrative genomics viewer. *Nat Biotechnol* 2011;**29**:24–6. https://doi.org/10.1038/nbt.1754
61. Buenrostro JD, Wu B, Chang HY *et al.* ATAC-seq: a method for assaying chromatin accessibility genome-wide. *Curr Protoc Mol Biol* 2015;**109**:21.29.1–9. https://doi.org/10.1002/0471142727.mb2129s109
62. Kereuger F, James F, Ewels P *et al.* FelixKrueger/TrimGalore: v0.6.10 - add default decompression path (0.6.10). Zenodo 2023; https://doi.org/10.5281/zenodo.7598955
63. Patro R, Duggal G, Love MI *et al.* Salmon provides fast and bias-aware quantification of transcript expression. *Nat Methods* 2017;**14**:417–9. https://doi.org/10.1038/nmeth.4197
64. Tian B, Li X, Kalita M *et al.* Analysis of the TGFbeta-induced program in primary airway epithelial cells shows essential role of NF-kappaB/RelA signaling network in type II epithelial mesenchymal transition. *BMC Genomics* 2015;**16**:529. https://doi.org/10.1186/s12864-015-1707-x
65. Tian B, Patrikeev I, Ochoa L *et al.* NF-kappaB mediates mesenchymal transition, remodeling, and pulmonary fibrosis in response to chronic inflammation by viral RNA patterns. *Am J Respir Cell Mol Biol* 2017;**56**:506–20. https://doi.org/10.1165/rcmb.2016-0259OC
66. Zhao Y, Jamaluddin M, Zhang Y *et al.* Systematic analysis of cell-type differences in the epithelial secretome reveals insights into the pathogenesis of respiratory syncytial virus-induced lower respiratory tract infections. *J Immunol* 2017;**198**:3345–64. https://doi.org/10.4049/jimmunol.1601291
67. Liu X, Salokas K, Tamene F *et al.* An AP-MS- and BioID-compatible MAC-tag enables comprehensive mapping of protein interactions and subcellular localizations. *Nat Commun* 2018;**9**:1188. https://doi.org/10.1038/s41467-018-03523-2
68. Bagchi S, Fredriksson R, Wallén-Mackenzie Å. *In situ* proximity ligation assay (PLA). *Methods Mol Biol* 2015;**1318**:149–59. https://doi.org/10.1007/978-1-4939-2742-5_15
69. Tian B, Yang J, Zhao Y *et al.* BRD4 couples NF-kappaB/RelA with airway inflammation and the IRF-RIG-I amplification loop in respiratory syncytial virus infection. *J Virol* 2017;**91**:e00007-17. https://doi.org/10.1128/JVI.00007-17
70. Liu Z, Chen H, Wang P *et al.* Discovery of orally bioavailable chromone derivatives as potent and selective BRD4 inhibitors: scaffold hopping, optimization, and pharmacological evaluation. *J Med Chem* 2020;**63**:5242–56. https://doi.org/10.1021/acs.jmedchem.0c00035

71. Kalluri R, Weinberg RA. The basics of epithelial–mesenchymal transition. *J Clin Invest* 2009;**119**:1420–8. https://doi.org/10.1172/JCI39104
72. Pastushenko I, Brisebarre A, Sifrim A *et al.* Identification of the tumour transition states occurring during EMT. *Nature* 2018;**556**:463–8. https://doi.org/10.1038/s41586-018-0040-3
73. Lee HS, Park JH, Kim SJ *et al.* A cooperative activation loop among SWI/SNF, gamma-H2AX and H3 acetylation for DNA double-strand break repair. *EMBO J* 2010;**29**:1434–45. https://doi.org/10.1038/emboj.2010.27
74. Creyghton MP, Cheng AW, Welstead GG *et al.* Histone H3K27ac separates active from poised enhancers and predicts developmental state. *Proc Natl Acad Sci USA* 2010;**107**:21931–6. https://doi.org/10.1073/pnas.1016071107
75. Lovén J, Hoke HA, Lin CY *et al.* Selective inhibition of tumor oncogenes by disruption of super-enhancers. *Cell* 2013;**153**:320–34. https://doi.org/10.1016/j.cell.2013.03.036
76. Lim S, Jin K, Friedman E. Mirk protein kinase is activated by MKK3 and functions as a transcriptional activator of HNF1alpha. *J Biol Chem* 2002;**277**:25040–6. https://doi.org/10.1074/jbc.M203257200
77. Ohtani K, Suzuki Y, Eda S *et al.* Molecular cloning of a novel human collectin from liver (CL-L1)*. *J Biol Chem* 1999;**274**:13681–9. https://doi.org/10.1074/jbc.274.19.13681
78. Huang J, Li J, Li Y *et al.* Interferon-inducible lncRNA IRF1-AS represses esophageal squamous cell carcinoma by promoting interferon response. *Cancer Lett* 2019;**459**:86–99. https://doi.org/10.1016/j.canlet.2019.05.038
79. Barriocanal M, Prats-Mari L, Razquin N *et al.* ISR8/IRF1-AS1 is relevant for IFNalpha and NF-kappaB responses. *Front Immunol* 2022;**13**:829335. https://doi.org/10.3389/fimmu.2022.829335
80. Ma H, Hu T, Tao W *et al.* A lncRNA from an inflammatory bowel disease risk locus maintains intestinal host-commensal homeostasis. *Cell Res* 2023;**33**:372–88. https://doi.org/10.1038/s41422-023-00790-7
81. Liesman RM, Buchholz UJ, Luongo CL *et al.* RSV-encoded NS2 promotes epithelial cell shedding and distal airway obstruction. *J Clin Invest* 2014;**124**:2219–33. https://doi.org/10.1172/JCI72948
82. Zhang L, Peeples ME, Boucher RC *et al.* Respiratory syncytial virus infection of human airway epithelial cells is polarized, specific to ciliated cells, and without obvious cytopathology. *J Virol* 2002;**76**:5654–66. https://doi.org/10.1128/JVI.76.11.5654-5666.2002
83. Yamane D, Feng H, Rivera-Serrano EE *et al.* Basal expression of interferon regulatory factor 1 drives intrinsic hepatocyte resistance to multiple RNA viruses. *Nat Microbiol* 2019;**4**:1096–104. https://doi.org/10.1038/s41564-019-0425-6
84. Cui K, Tailor P, Liu H *et al.* The chromatin-remodeling BAF complex mediates cellular antiviral activities by promoter priming. *Mol Cell Biol* 2004;**24**:4476–86. https://doi.org/10.1128/MCB.24.10.4476-4486.2004
85. Barutcu AR, Lajoie BR, Fritz AJ *et al.* SMARCA4 regulates gene expression and higher-order chromatin structure in proliferating mammary epithelial cells. *Genome Res* 2016;**26**:1188–201. https://doi.org/10.1101/gr.201624.115
86. Dey A, Chitsaz F, Abbasi A *et al.* The double bromodomain protein Brd4 binds to acetylated chromatin during interphase and mitosis. *Proc Natl Acad Sci USA* 2003;**100**:8758–63. https://doi.org/10.1073/pnas.1433065100
87. Zou Z, Huang B, Wu X *et al.* Brd4 maintains constitutively active NF-κb in cancer cells by binding to acetylated RelA. *Oncogene* 2014;**33**:2395–404. https://doi.org/10.1038/onc.2013.179
88. Brown JD, Lin CY, Duan Q *et al.* NF-κb directs dynamic super enhancer formation in inflammation and atherogenesis. *Mol Cell* 2014;**56**:219–31. https://doi.org/10.1016/j.molcel.2014.08.024
89. Skibba ME, Xu X, Weiss K *et al.* Role of Secretoglobin(+) (club cell) NFκB/RelA-TGFβ signaling in aero-allergen-induced epithelial plasticity and subepithelial myofibroblast transdifferentiation. *Respir Res* 2021;**22**:315. https://doi.org/10.1186/s12931-021-01910-w
90. Zheng X, Wang K, Pan L *et al.* Innate immune responses to RSV infection facilitated by OGG1, an enzyme repairing oxidatively modified DNA base lesions. *J Innate Immun* 2022;**14**:593–614.
91. Zhang J, Jamaluddin M, Zhang Y *et al.* Type II epithelial–mesenchymal transition upregulates protein N-glycosylation to maintain proteostasis and extracellular matrix production. *J Proteome Res* 2019;**18**:3447–60. https://doi.org/10.1021/acs.jproteome.9b00342
92. Tian B, Zhao Y, Sun H *et al.* BRD4 mediates NFkB-dependent epithelial–mesenchymal transition and pulmonary fibrosis via transcriptional elongation. *Am J Physiol Lung Cell Mol Physiol* 2016;**311**:L1183–201. https://doi.org/10.1152/ajplung.00224.2016
93. Devaiah BN, Lewis BA, Cherman N *et al.* BRD4 is an atypical kinase that phosphorylates serine2 of the RNA polymerase II carboxy-terminal domain. *Proc Natl Acad Sci USA* 2012;**109**:6927–32. https://doi.org/10.1073/pnas.1120422109
94. Mann M, Roberts DS, Zhu Y *et al.* Discovery of RSV-induced BRD4 protein interactions using native immunoprecipitation and parallel accumulation-serial fragmentation (PASEF) mass spectrometry. *Viruses* 2021;**13**:454. https://doi.org/10.3390/v13030454
95. Tian B, Zhao Y, Kalita M *et al.* CDK9-dependent transcriptional elongation in the innate interferon-stimulated gene response to respiratory syncytial virus infection in airway epithelial cells. *J Virol* 2013;**87**:7075–92. https://doi.org/10.1128/JVI.03399-12
96. Brasier AR. Orchestrating epigenetic readers: progress in understanding the functions of bromodomain-containing protein 4 complexes. *Mol Ther Nucleic Acids* 2023;**32**:340–2. https://doi.org/10.1016/j.omtn.2023.03.024
97. Mann MW, Fu Y, Gearhart RL *et al.* Bromodomain-containing protein 4 regulates innate inflammation via modulation of alternative splicing. *Front Immunol* 2023;**14**:1212770. https://doi.org/10.3389/fimmu.2023.1212770
98. Xu X, Mann M, Qiao D *et al.* Alternative mRNA processing of innate response pathways in respiratory syncytial virus (RSV) infection. *Viruses* 2021;**13**:218. https://doi.org/10.3390/v13020218
99. Imamura K, Imamachi N, Akizuki G *et al.* Long noncoding RNA NEAT1-dependent SFPQ relocation from promoter region to paraspeckle mediates IL8 expression upon immune stimuli. *Mol Cell* 2014;**53**:393–406. https://doi.org/10.1016/j.molcel.2014.01.009
100. Feng H, Zhang Y-B, Gui J-F *et al.* Interferon regulatory factor 1 (IRF1) and anti-pathogen innate immune responses. *PLoS Pathog* 2021;**17**:e1009220. https://doi.org/10.1371/journal.ppat.1009220

Received: October 1, 2024. **Revised:** February 25, 2025. **Editorial Decision:** February 28, 2025. **Accepted:** March 6, 2025